

8-2012

Synthesis and Characterization of Biodegradable Electrospun Polyurethanes For Biomedical Applications

Xujun Zhang
University of Texas-Pan American

Follow this and additional works at: https://scholarworks.utrgv.edu/leg_etd

 Part of the [Chemistry Commons](#)

Recommended Citation

Zhang, Xujun, "Synthesis and Characterization of Biodegradable Electrospun Polyurethanes For Biomedical Applications" (2012). *Theses and Dissertations - UTB/UTPA*. 552.
https://scholarworks.utrgv.edu/leg_etd/552

This Thesis is brought to you for free and open access by ScholarWorks @ UTRGV. It has been accepted for inclusion in Theses and Dissertations - UTB/UTPA by an authorized administrator of ScholarWorks @ UTRGV. For more information, please contact justin.white@utrgv.edu, william.flores01@utrgv.edu.

SYNTHESIS AND CHARACTERIZATION
OF BIODEGRADABLE ELECTROSPUN POLYURETHANES
FOR BIOMEDICAL APPLICATIONS

A Thesis

by

XUJUN ZHANG

Submitted to the Graduate School of the
University of Texas-Pan American
In partial fulfillment of the requirements for the degree of
MASTER OF SCIENCE

August 2012

Major Subject: Chemistry

SYNTHESIS AND CHARACTERIZATION
OF BIODEGRADABLE ELECTROSPUN POLYURETHANES
FOR BIOMEDICAL APPLICATIONS

A Thesis
by
XUJUN ZHANG

COMMITTEE MEMBERS

Dr. Javier Macossay-Torres
Chair of Committee

Dr. Bimal K. Banik
Committee Member

Dr. Elamin E. Ibrahim
Committee Member

Dr. Narayan Bhat
Committee Member

August 2012

Copyright 2012 Xujun Zhang
All Rights Reserved

ABSTRACT

Zhang Xujun, Synthesis and Characterization of Biodegradable Electrospun Polyurethanes for Biomedical Applications. Master of Science (MS), August, 2012, 92 pp., 18 tables, 29 figures, 10 schemes, 53 reference, 33 titles.

Two types of polyesters [(Poly(ϵ -caprolactone) and Poly(δ -valerolactone)] were synthesized by ring-opening polymerization with diethylene glycol as a initiator and stannous octate as a catalyst. The corresponding polyurethanes were synthesized by two-step polymerization with 1,4-diisocyanate butane (BDI) and reacted with 1,4-diamino butane (Putrescine) chain extender. The polymers were characterized by Proton Nuclear Magnetic Resonance (^1H NMR), Fourier Transform Infrared Spectroscopy (FT-IR), Raman Spectroscopy, Size-exclusive Chromatography (SEC), Thermogravimetric Analysis (TGA) and Differential Scanning Calorimetry (DSC). The resulting polyurethanes were fabricated into nanofibers using an electrospinning technique. The morphological, structural characterizations and thermal properties of the bulk polyurethanes and electrospun polyurethanes nanofibers were analyzed by Scanning Electron Microscopy (SEM), FT-IR, Raman, TGA and DSC. The degradability of electrospun polyurethane nanofibers were investigated in phosphate buffer solution (pH=7.2) at 37 °C at a period of 5 days.

DEDICATION

The completion of my master studies would not have been possible without the love and support of my family. My father, Anxin Xu, my mother, Chunmei Zhang, wholeheartedly inspired, motivated and supported me by all means to accomplish this degree. Thank you for your love and patience.

ACKNOWLEDGEMENTS

I would like to express my gratitude to Dr. Javier Macossay-Torres, chair of my thesis committee, for all his mentoring and advice. My thanks go to my thesis committee members: Dr. Elamin E. Ibrahim, Dr. Bimal K. Banik, and Dr. Narayan Bhat for their advice and comments on my thesis.

I would also like to thank Dr. Sheikh Faheem Arjamend and Travis Cantu for their encouragement and support.

TABLE OF CONTENTS

	Page
ABSTRACT.....	iii
DEDICATION.....	iv
ACKNOWLEDGEMENTS.....	v
TABLE OF CONTENTS.....	vi
LIST OF TABLES.....	xi
LIST OF FIGURES.....	xiii
LIST OF SCHEMES.....	xv
CHAPTER I. INTRODUCTION.....	1
1.1 Brief introduction to anterior cruciate ligament (ACL).....	1
1.1.1 Traditional treatments.....	1
1.1.2 Tissued-engineered ACLs.....	3
1.2 Polyurethanes.....	5
1.2.1 Basic chemistry of polyurethanes.....	5

1.2.2 Raw materials	7
1.2.2.1 Isocyanate	7
1.2.2.2 Polyols	8
1.2.2.3 Chain extenders.....	9
1.2.3 Synthesis of polyurethanes.....	10
1.2.4 Hydrogen bonding and mechanical properties.....	11
1.2.5 Biomedical applications	12
1.3 Electrospinning.....	13
1.3.1 History of electrospinning and production of nanofibers.....	14
1.3.2 Electrospun polymeric nanofibers for tissue engineering.....	15
1.4 Research plan	17
1.4.1 Project description	17
1.4.2 Objectives	18
CHAPTER II. SYNTHESIS OF POLYCAPROLACTONE (PCL), POLYVALEROLACTONE (PVL) AND CORRESPONDING POLYURETHANES	21
2.1 Introduction	21
2.2 Materials and Methods	22
2.2.1 Materials.....	22

2.2.2	Synthesis of polyols	23
2.2.3	Synthesis of polyurethanes	24
2.3	Characterizations	26
2.3.1	Proton Nuclear Magnetic Resonance (^1H NMR)	26
2.3.2	Fourier Transform Infrared Spectroscopy (FT-IR)	26
2.3.3	Raman spectroscopy.....	27
2.3.4	Size-exclusive Chromatography (SEC)	27
2.3.5	Thermogravimetric Analysis (TGA)	27
2.3.6	Differential Scanning Calorimetry (DSC)	28
2.4	Results and Discussions	28
2.4.1	Synthesis of PCL, PVL, PU-PCL and PU-PVL.....	28
2.4.2	^1H NMR.....	30
2.4.3	FT-IR	36
2.4.4	Raman.....	40
2.4.5	SEC.....	44
2.4.6	TGA.....	48
2.4.7	DSC	51
CHAPTER III. ELECTROSPINNING OF BIODEGRADABLE POLYURETHANES.....		56

3.1	Introduction	56
3.2	Materials and Methods	58
3.2.1	Materials.....	58
3.2.2	Electrospinning process of PU-PCL and PU-PVL.....	58
3.3	Characterizations	59
3.3.1	Scanning Electron Microscopy (SEM)	59
3.3.2	Fourier Transform Infrared Spectroscopy (FT-IR).....	60
3.3.3	Raman spectroscopy.....	60
3.3.4	Thermogravimetric Analysis (TGA)	60
3.3.5	Differential Scanning Calorimetry (DSC)	60
3.3.6	Degradation behavior	61
3.4	Results and Discussions	61
3.4.1	Electrospinning parameters.....	61
3.4.2	SEM.....	62
3.4.3	FT-IR spectra.....	65
3.4.4	Raman spectra	66
3.4.5	TGA.....	68
3.4.6	DSC	69

3.4.7 Degradation of electrospun polyurethanes	70
CHAPTER IV. CONCLUSIONS AND FUTURE WORK	76
4.1 Conclusions	76
4.2 Future work	77
REFERENCES	79
APPENDIX A	84
BIOGRAPHICAL SKETCH	92

LIST OF TABLES

	Page
Table 1.1: The advantages and disadvantages of the three types of grafts are shown.	3
Table 1.2: The main requirements of a scaffold with respect to their application are shown..	5
Table 1.3: Commonly used isocyanates for producing polyurethanes are shown.	8
Table 1.4: Typical polyols are used in synthesis of polyurethanes.	9
Table 1.5: Typical examples of chain extenders are shown.	10
Table 2.1: Synthesis conditions of PCL and PVL polyols.	28
Table 2.2: Synthesis conditions of PU-PCL and PU-PVL.	29
Table 2.3: Number-average of molecular weights of synthesized polyols.	36
Table 2.4: Characteristic FT-IR peaks assignments of PCL.	38
Table 2.5: Characteristic FT-IR peaks assignments of PU-PCL.	39
Table 2.6: Characteristic peaks assignment for CL and PCL.	43
Table 2.7: SEC results of synthesized polyols and polyurethanes.	45
Table 2.8: Onset decomposition temperatures for PCL, PU-PCL, PVL and PU-PVL.	48
Table 2.9: DSC data of PCL, PU-PCL, PVL and PU-PVL.	54
Table 3.1: Electrospinning conditions of PU-PCL and PU-PVL polymers.	62

Table 3.2: Characteristic peak assignments for Raman spectrum of electrospun PU-PCL... 68	68
Table 3.3: Electrospun PU-PCLs (A, B and C) were immersed in 4M NaOH before placing into phosphate buffer..... 71	71
Table 3.4: Electrospun PU-PCLs (E, F and G) were in Phosphate buffer. 73	73

LIST OF FIGURES

	Page
Figure 1.1: The main knee ligaments are located around and within the knee joint.	2
Figure 1.2: Possible hydrogen bonding interaction in polyurethanes.....	12
Figure 1.3: Diagram representing the components of a typical electrospinning set-up.....	13
Figure 1.4: Diagram shows the electrospinning set-up.....	14
Figure 1.5: SEM images of the nanofiber mats showing cell attachments after 4 days of culturing cells for the prepared silver NPs/PU nanofiber matrices: 0% (A), 2% (B), 5% (C), 7% (D), and 10% (E). The inset in each figure shows high magnification image...	16
Figure 2.1: ^1H NMR spectrum of synthesized PCL 20:1.....	31
Figure 2.2: ^1H NMR spectrum of synthesized PVL 20:1.	33
Figure 2.3: ^1H NMR spectrum of synthesized PU-PCL 20:1.	35
Figure 2.4: FTIR spectra of synthesized PCL and PU-PCL.	37
Figure 2.5: FTIR spectra of synthesized PVL and PU-PVL.....	40
Figure 2.6: Raman spectra of diethylene glycol, putrescine, and 1,4-diisocyanate (BDI). ...	41
Figure 2.7: Raman spectra of CL, PCL and PU-PCL.	42

Figure 2.8: Raman spectra of VL, PVL and PU-PVL.....	44
Figure 2.9: Overlay of SEC curves for PCL (20:1 and 40:1) and PVL (20:1 and 40:1).....	46
Figure 2.10: SEC curves of polyurethane prepared from PVL 20:1.....	47
Figure 2.11: TGA curves of PCL (20:1 and 40:1) and PU-PCL 20:1.	50
Figure 2.12: TGA curves of PVL (20:1 and 40:1) and PU-PVL 20:1.	51
Figure 2.13: DSC of (a) PCL 20:1, (b) PCL 40:1, (c) PU-PCL 20:1.	53
Figure 2.14: DSC of (a) PVL 20:1, (b) PVL 40:1, (c) PU-PVL 20:1.	55
Figure 3.1: SEM micrographs of 10 % (w/v) of PU-PCL nanofibers.....	63
Figure 3.2: SEM micrographs of 15% (w/v) of PU-PCL nanofibers.....	64
Figure 3.3: SEM micrographs of 20% (w/v) of PU-PVL after electrospinning.	65
Figure 3.4: FT-IR spectra of bulk PU-PCL and electrospun PU-PCL.	66
Figure 3.5: Raman spectra of bulk PU-PCL and electrospun PU-PCL.	67
Figure 3.6: TGA curves of PU-PCL 20:1 and electrospun PU-PCL 20:1.....	69
Figure 3.7: DSC curves of electrospun PU-PCL 20:1.	70
Figure 3.8: Degradation curves of electrospun PU-PCLs in phosphate buffer (pH=7.2) at 37 °C. All values are mean \pm SD, $n=3$	72
Figure 3.9: Degradation of electrospun PU-PCLs (A, B and C) immersed in 4M NaOH before placing into phosphate buffer (pH=7.2) at 37 °C. All values are mean \pm SD, $n=3$	74
Figure 3.10: Degradation of electrospun PU-PCLs (E, F and G) placing into phosphate buffer (pH=7.2) at 37 °C. All values are mean \pm SD, $n=3$	75

LIST OF SCHEMES

	Page
Scheme 1.1: General synthesis of a polyurethane.	6
Scheme 1.2: Formations of urethane linkage (a) and urea linkage (b) are shown.	6
Scheme 1.3: Mechanism of formations of urethane (a) and urea linkage (b).	7
Scheme 1.4: Syntheses of polyurethanes by two-step process.	11
Scheme 1.5: Synthesis of polyvalerolactone diol and polycaprolactone diol.	18
Scheme 1.6: Synthesis of polyurethane ureas based on PCL or PVL polyols.	19
Scheme 2.1: Mechanism of Ring-Opening Polymerization of caprolactone under stannous octate catalyst, (a, b) formation of stannous alkoxide initiator, (c, d) generation of 1mer and polymer, and (e) chain-end deactivation by reacting with water.	23
Scheme 2.2: Synthesis of polyvalerolactone (a) and polycaprolactone (b) using diethylene glycol as initiator and stannous octate as catalyst.	24
Scheme 2.3: Synthesis of polyurethane by two-step process using BDI and Putrescine.	25
Scheme 3.1: The electrospinning set-up.	59

CHAPTER I

INTRODUCTION

1.1 Brief introduction to the anterior cruciate ligament

The anterior cruciate ligament (ACL) tears have become the most common injuries of the knees at present times. It is estimated that there are between 100,000 and 250,000 (or 1 in 3,000 in the general population) patients per year diagnosed with ACL disruptions ^[1]. It is also believed that the most important function for ACL is to give support and strength to the knee and simultaneously prevent extreme translation of the tibia relative to the femur (Figure 1.1). After rupture of this important ligament, the usual process required is to have surgery, which often leads to defected movement of body parts ^[2].

1.1.1 Traditional treatments

As mentioned, ACL injuries are becoming a growing problem, and there are a number of treatment options available. This includes the replacement of torn/worn ACL or by creating ACL reconstruction procedures ^[2]. For example, autografts, allografts and synthetic devices are the most traditional methods that surgeons follow. However, each of the three surgical procedures has its own advantages and disadvantages (Table 1.1). Among them, autografting is the current gold standard procedure for reconstructing an ACL, which involves using a ligament or tendon

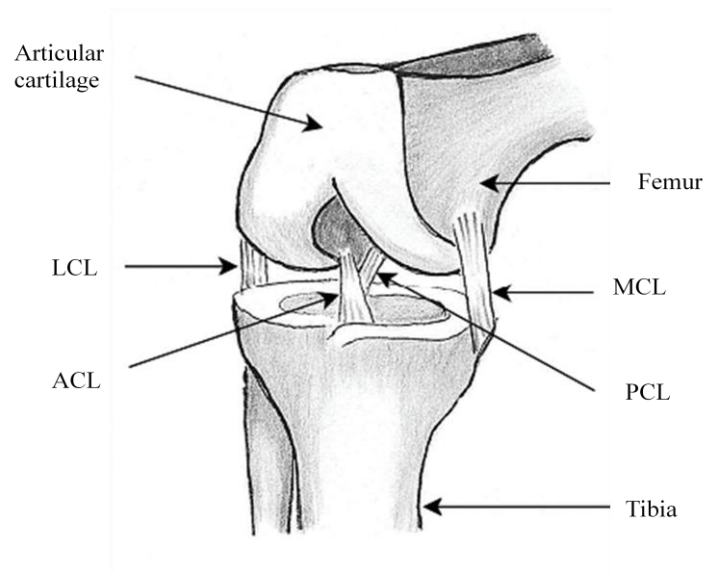


Figure 1.1 The main knee ligaments are located around and within the knee joint ^[3].

from another part of the patient's own body and using it to replace the damaged ACL. Allografting is the procedure that uses a ligament or tendon from a different human donor. Neither the autograft nor the allograft have satisfied long term performance in some patients due to the key factor, which is shortage of graft, allergic reactions and mechanical failures ^[3].

Also, in the past, many attempts have been made to use synthetic materials for ACL replacements, such as non-degradable polyethylene, polypropylene and poly (tetrafluoroethylene). Although these synthetic devices have typically a functional performance in short term, they fail over time which result in permanent deformation ^[4].

Table 1.1 The advantages and disadvantages of the three types of grafts are shown ^[3].

	Advantages	Disadvantages
Autograft	<p>No rejection</p> <p>No disease transmission</p> <p>No donor scarcity</p>	<p>Donor site morbidity, Patellar fracture, Quadriceps weakness, Limited bone integration, Mismatch in different tissue properties; causing mechanical failure, creeping, fatigue, recurring injury</p>
Allograft	<p>No donor site morbidity</p>	<p>Donor scarcity, Limited bone integration, Tissue rejection, Mismatch in different tissue properties; causing mechanical failure, creeping, fatigue, recurring injury</p>
Synthetic devices	<p>No donor site morbidity</p> <p>No tissue disease transmission</p> <p>No donor scarcity</p>	<p>Limited bone integration (weak graft-host tissue interface), Mismatch in different tissue properties; causing mechanical failure, creeping (stretching & loosening), Poor long-term instability, fatigue, recurring injury</p>

1.1.2 Tissue-engineered ACLs

In order to overcome the limitations of the current treatments, many researchers have been studying new materials and technologies that display similar mechanical properties to that of natural ACL. In this regard, tissue engineering has evolved as the most popular and desirable approach in the field of ACL reconstruction. Tissue engineering is the application of biological, chemical and engineering principles to develop substitutes for the repair and restoration of tissue

functions^[5]. Some tissues in the body are able to self repair after injury, while others are not, and tissue engineering is a relatively new technique which could be an alternative method to repair damaged tissues. Usually, the procedure involves using a scaffold to act as a structural support for cell growth and eventually generate a functional tissue.

Therefore, a tissue-engineered scaffold is required to meet certain requirements (Table 1.2). For example, it has to be biocompatible, biodegradable, allow cell adherence, have sufficient surface area and volume for cell in-growth, be sufficiently strong to withstand mechanical loading forces *in-vitro* and *in-vivo*, and possess a similar stiffness to that of native ligament present in human body^[6-9]. Currently, various materials have been investigated for use in tissue-engineered ligament reconstructions, with polyurethanes showing the potential to be used for ACL replacement^[10].

Table 1.2 The main requirements of a scaffold with respect to their application are shown ^[3].

Scaffold requirements	The purpose of this feature
Biocompatible	Avoids immune-rejection (a cytotoxic response could kill the cells)
Biodegradable	To degrade at the same rate at which neotissue forms to avoid the need for surgical removal
Enable cell adherence	To allow cells attachment for growth and proliferation to occur
Provide sufficient surface area/volume	To provide sufficient space for cell spreading and growth
Posses compatible strength/stiffness	To withstand cyclic mechanical loading forces with magnitudes and strains similar to those found in vivo
Surgical implantation	Ease of fixing/bonding to bone (bio-active)

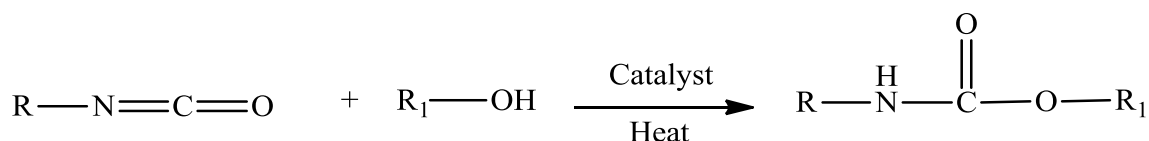
1.2 Polyurethanes

Polyurethane is a general name for a class of polymers that have the basic urethane moiety in their chemical structure. In 1937, polyurethanes were first produced and investigated by Dr. Otto Bayer and coworkers ^[11]. After 1937, these polymers have been widely used in many fields, such as in medical, automotive and industrial applications ^[11].

1.2.1 Basic chemistry of polyurethanes

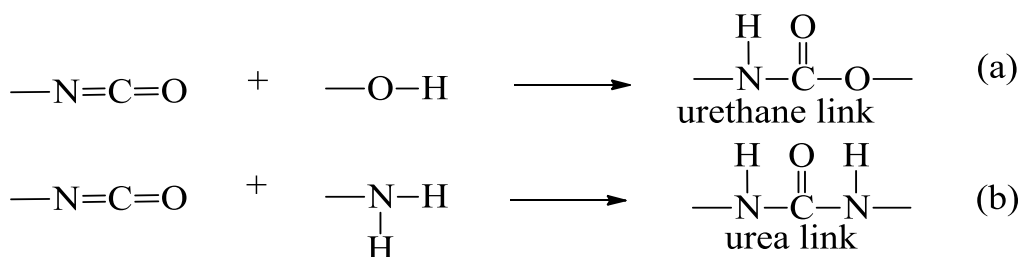
Polyurethanes are typically a linear or cross linked polymers that have repeating units of urethane group. The urethane group (-NHCO₂-) is generated by an addition reaction between a

diisocyanate and a polyol (Scheme 1.1). The diisocyanate is a low molecular weight compound that can react with either the polyol or chain extender. The chain extender is usually a small molecule with either hydroxyl, or amine terminated groups. The polyol with long and flexible chain is always called as soft segment. These soft segments can also be derived from a hydroxyl terminated aliphatic or aromatic polyester, polyether or polyalkene.



Scheme 1.1 General synthesis of a polyurethane.

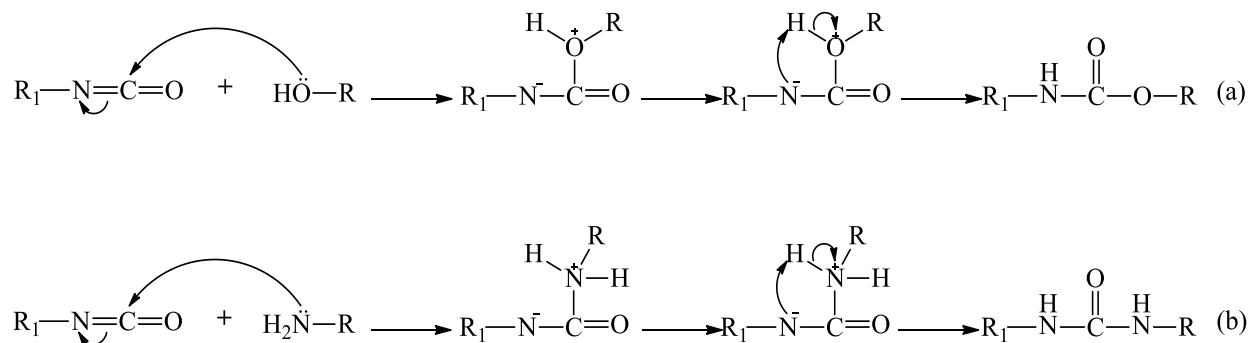
The principle chemical reaction involved in the synthesis of polyurethanes is the urethane linkage formation, i.e., the reaction between isocyanate and hydroxyl groups. The hydrogen atom of the hydroxyl or amine group is transferred to the nitrogen atom of the diisocyanate, to form urethane linkage (Scheme 1.2).



Scheme 1.2 Formations of urethane linkage (a) and urea linkage (b) are shown.

Another important basic step is the chain extension reaction which occurs between the chain extender (usually diol or diamine) and the isocyanate. When a diol is used as a chain extender, urethane will be formed according to (Scheme 1.2a), while urea will be formed according to (Scheme 1.2b) if diamine is used. The segments produced by the reaction of an isocyanate and a

diol or a diamine are also called hard segments. The mechanism of urethane or urea linkage formation is shown in the following (Scheme 1.3).

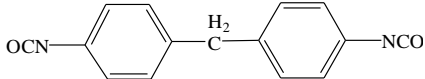
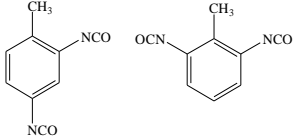
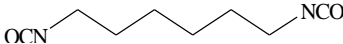


Scheme 1.3 Mechanism of formations of urethane (a) and urea linkage (b).

1.2.2 Raw materials

1.2.2.1 Isocyanate. In polyurethane synthesis, the mostly used monomer is the diisocyanate, containing two isocyanate groups at the terminal end. Usually, diisocyanates can be either aliphatic or aromatic forms of monomers (Table 1.3). Among them, 4,4'-diphenylmethane diisocyanate (MDI) and toluenemethyl diisocyanate (TDI) are most commonly used aromatic diisocyanates ^[12]. Isocyanates can react easily with groups containing active hydrogen atoms because of their highly reactive nature, for example, the side reaction between an isocyanate and water can easily occur, which has to be avoided during the synthesis of polyurethanes.

Table 1.3 Commonly used isocyanates for producing polyurethanes are shown.

Isocyanate	Structure
4,4'-diphenylmethane diisocyanate (MDI)	
Toluenemethyl diisocyanate (TDI)	
1,6-hexamethylene diisocyanate (HDI)	

1.2.2.2 Polyols. Polyols are hydroxyl terminated group compounds with molecular weights ranging from a few hundred to a few thousand units. Due to the various molecular weights, polyols exhibit different physical states, which can be either liquid or solid (wax-like) at room temperature. A wide range of polyols have been investigated for the manufacture of polyurethanes. However, most of them can be classified as two types: hydroxyl terminated polyesters and hydroxyl polyethers. Polyesters are prepared by polyesterification of dicarboxylic acids with diols. Also, polyesters derived from ϵ -caprolactone, hydroxyl-terminated aliphatic and cycloaliphatic polycarbonates have been widely used for synthesis of polyurethanes. Polyether diols are generally produced by the addition of alkylene oxides to alcohols or amines, which are called initiators, and by ring-opening polymerization of tetrahydrofuran. Typical polyols are listed in (Table 1.4).

Table 1.4 Typical polyols are used in synthesis of polyurethanes ^[11].

Polyols	Structure
Polyethylene oxide (PEO)	HO-(CH ₂ CH ₂ -O) _n -H
Polytetramethylene oxide (PTMO)	HO-(CH ₂ CH ₂ CH ₂ CH ₂ -O) _n -H
Polycaprolactone (PCL)	HO-[(CH ₂) ₅ -CO-O] _n -H
Polyethylene adipate (PEA)	HO-[(CH ₂) ₄ -O-OC(CH ₂)CO-O] _n -H

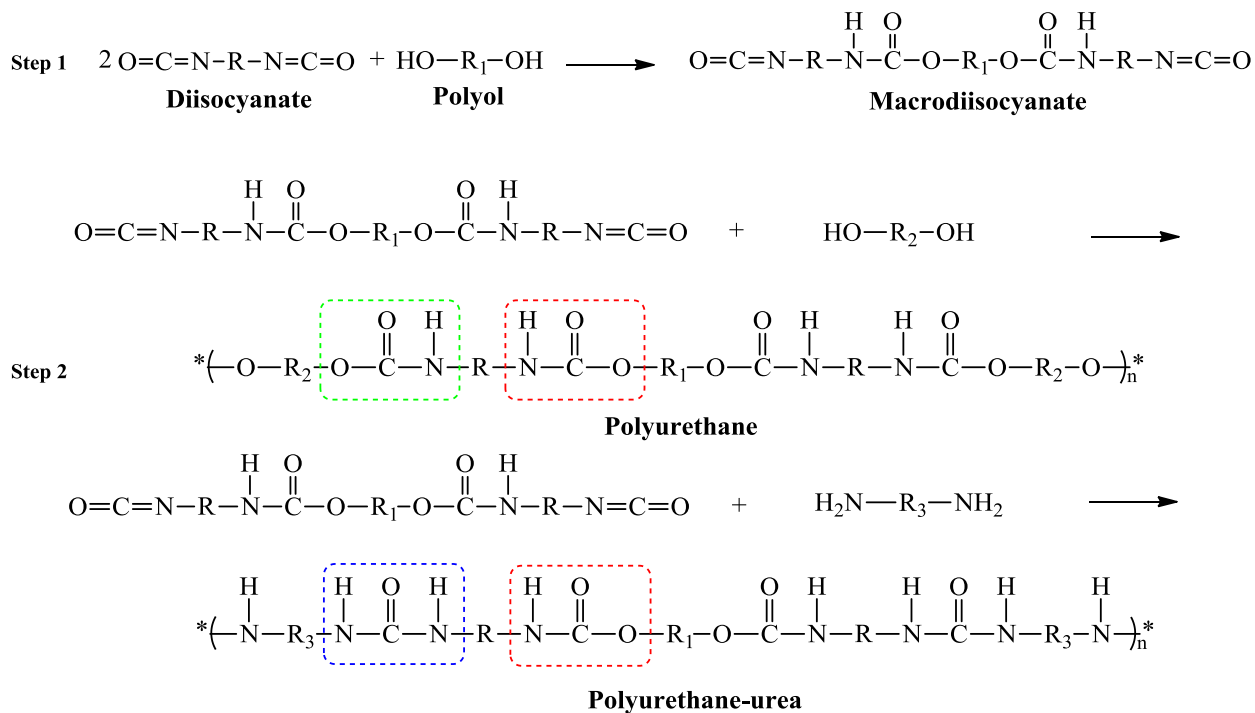
1.2.2.3 Chain extenders. A number of compounds with hydroxyl or amine terminated group can be used as chain extenders in the synthesis of polyurethanes. As a part of the hard segments, chain extenders play an important role in producing and extending the length of polyurethane molecules, which results in the dramatic increase of the molecular weights of polyurethanes. Due to this, the mechanical strength of polyurethanes can be drastically improved. In general, polyurethanes prepared with diamines as chain extenders usually have better physical properties than the ones prepared with diols ^[12]. Also, polyurethanes synthesized with aromatic chain extenders are stiffer than those synthesized with aliphatic ones. It is studied that the use of aliphatic chain extender with an even number of backbone carbon atoms, results in better mechanical properties than with an odd number of backbone carbon atoms. This seems to be explained by the better crystalline order within hard segments ^[12]. Typical examples of chain extenders are shown in Table 1.5.

Table 1.5 Typical examples of chain extenders are shown ^[11].

Chain Extender	Structure
Diethylene glycol	HO-CH ₂ CH ₂ -O-CH ₂ CH ₂ -OH
1,4-butanediol	HO-CH ₂ CH ₂ CH ₂ CH ₂ -OH
Ethylene diamine	H ₂ N-CH ₂ CH ₂ -NH ₂

1.2.3 Synthesis of polyurethanes

Generally, there are two classified methods for polyurethane syntheses, these include one-step and two-steps, respectively ^[12]. The one-step process is also called one-shot method, which means all the reactants (polyol, isocyanate and chain extender) are added together initially and simultaneously. Then, the mixture is allowed to polymerize under vigorous stirring conditions. It's reported that the resulting polymer using the one-shot procedure has basically a random distribution of monomer units along the polymer chain ^[13]. To synthesize alternated polyurethanes, which have a linear distribution of monomers, a two-steps procedure is usually preferred ^[14]. First, a pre-polymer which has the isocyanate functional end groups is produced by the reaction of a polyol with the excess amount of diisocyanate. Then, the chain extender is added to form a high molecular weight polymer. In industry, commercial polyurethanes are obtained by using bulk solution polymerizations, namely the one-shot method. However, the two-steps method or prepolymer process is preferred in research laboratories because of the relative ease in controlling the reaction. The process of two-steps is illustrated in Scheme 1.4.



Scheme 1.4 Syntheses of polyurethanes by two-step process.

1.2.4 Hydrogen bonding and mechanical properties

Hydrogen bonding in polyurethanes plays an important role in determining their mechanical properties [12]. The formation of multiple hydrogen bonds results from the presence of urethane's N-H and urea's N-H groups acting as proton donors. Meanwhile, the hydrogen bond acceptors can be either urethane's C=O, urea's C=O groups in hard segments or ester (C=O) and ether (C-O-C) groups in soft segments. There are several possible hydrogen bonding sites appearing in polyurethanes (Figure 1.2). Different types of hydrogen bonds have relatively variable contribution to phase segregation. Those hydrogen bonds in hard segments domains have a significant influence on the mechanical behavior of the polyurethane. The hydrogen bonding interaction produces the formation of physical crosslinks, which results in the increase of

strength and stiffness ^[15].

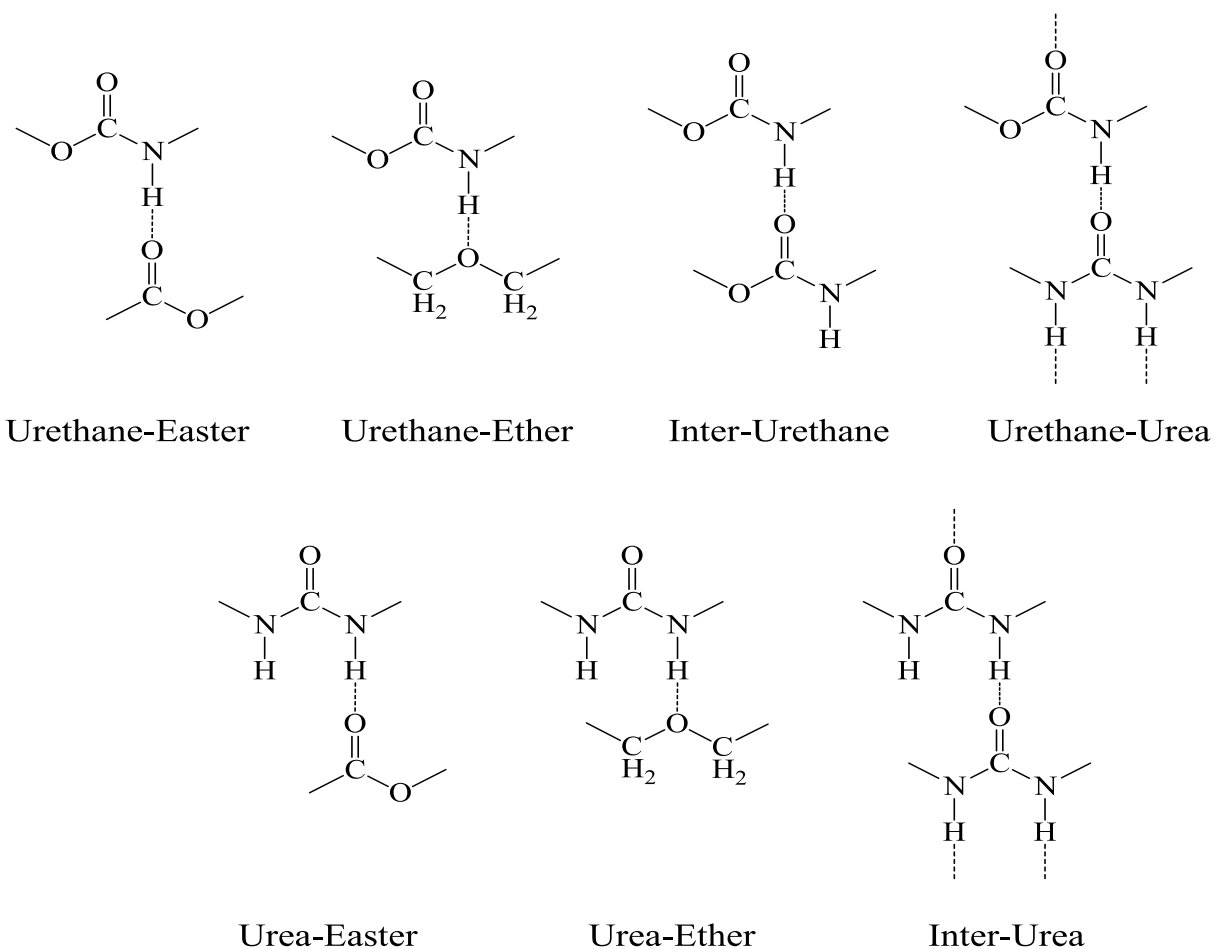


Figure 1.2 Possible hydrogen bonding interaction in polyurethanes.

1.2.5 Biomedical applications

Polyurethanes exhibit many excellent physical and chemical properties for biomedical applications. For instance, one of the characteristic properties of polyurethanes is the mechanical flexibility combined with higher tear strength. These desirable properties have gained tremendous interest in the development of applications for biomedical devices. The early biomedical applications of polyurethanes can be dated back to the 1960s. At that time, for

example, polyesterurethane foam was used for in-situ bone fixation ^[12,13]. While polyesterurethane coatings were applied to cardiovascular implants ^[12,13]. From that time, the research of polyurethanes for biomedical applications has increased intensively. Currently, polyurethanes have been explored in a number of biomedical tissue engineering applications, such as used as scaffolds for tissue ingrowths, breast implants and vascular grafts ^[13,14].

1.3 Electrospinning

Electrospinning is the most commonly used technique to produce nanofibers, which can be used as tissue scaffolds ^[16]. This technique allows producing polymer fibers with diameters varying from micrometer to nanometer levels ^[17,18]. Electrospinning is a unique method using electrostatic forces to produce fine fibers. The typical electrospinning set-up consists of a syringe pump, a high voltage source, and a collector (Figure 1.3).

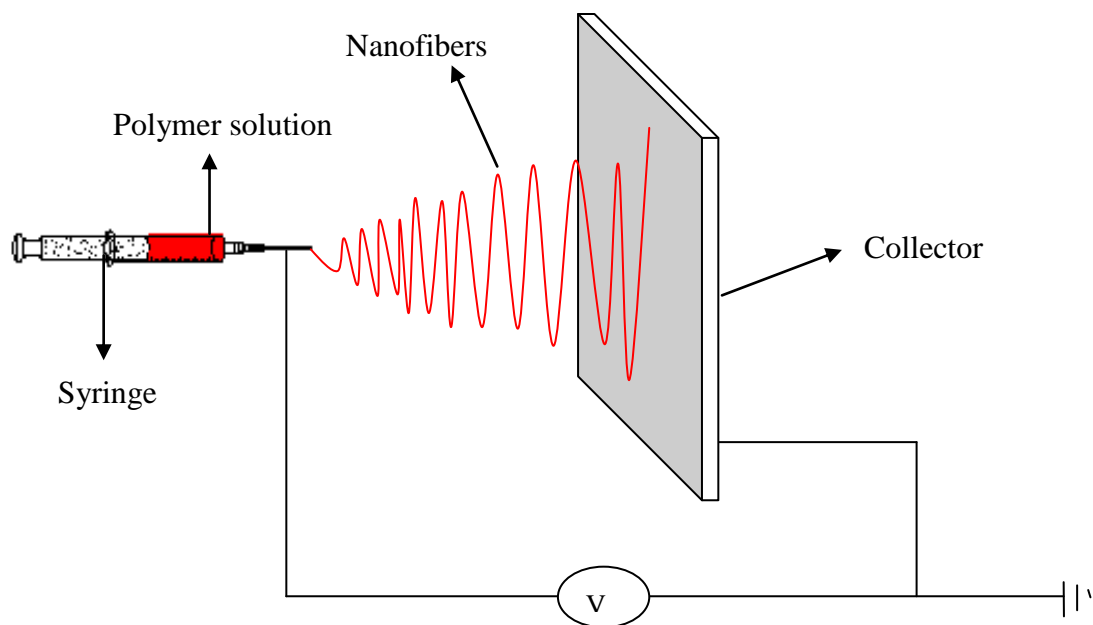


Figure 1.3 Diagram representing the components of a typical electrospinning set-up.

Generally, an optimum concentration of polymer solution is pumped at a constant rate using a syringe pump. The electric field is generated by connecting one electrode from the high voltage source to the needle and the other electrode to an opposite polarity collector (usually a grounded collector). When the high voltage, normally ranging from 5kV to 30kV is applied to the needle, the surface of the droplet held by its own surface tension gets electrostatically charged at the spinneret tip ^[18]. Once the electric field attains a certain critical value, the electrostatic forces overcome the surface tension of polymer solution, a conical shape known as the Taylor cone is produced. When the electric field is over than the critical value, the liquid jet continues to be ejected and elongated, while the solvent evaporates. The randomly oriented thin polymeric fibers are solidified and collected on the collector (Figure 1.4).

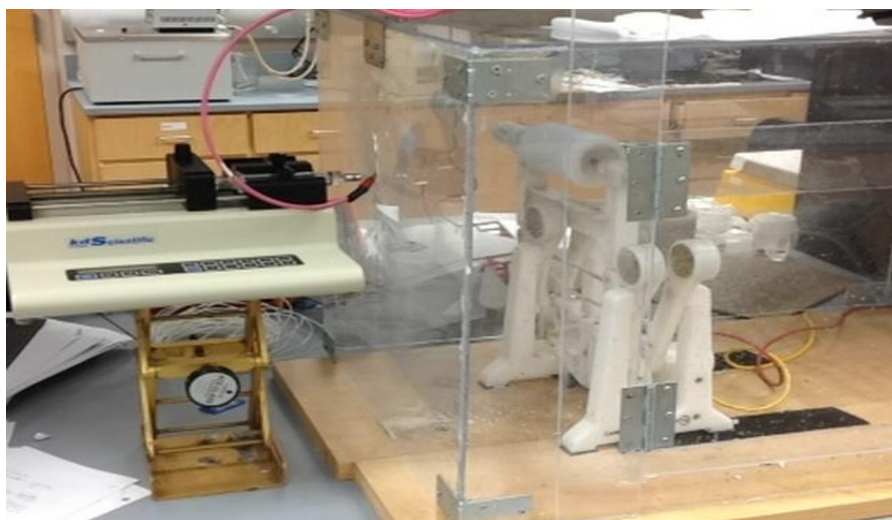


Figure 1.4 Diagram shows the electrospinning set-up.

1.3.1 History of electrospinning and production of nanofibers

The electrospinning process was first patented by J.F. Cooley and W.J. Morton in the early 1900s. In 1934, Aton and Formhals published a series of patents mentioning an experimental

set-up for the production of polymer filaments using an electrostatic force ^[19]. By 1969, Taylor developed a method that involved the jet produced from the droplet of a polymer solution, where he observed that an angle of 49.3 ° is obtained when the surface tension forces balanced the electric field ^[20]. The conical shape of the droplet was then referred to as the “Taylor cone” by other researchers. Very little further work on electrospinning was studied until the early 2000s. To date, electrospinning has gained a lot of popularity and attention in a wide range of biomedical and industrial applications, not only because electrospinning is easy to perform and produces nanofibers with a variety of properties, but it also provides some particular advantages such as high surface to volume ratio, and adjustable porosity of structures ^[18].

1.3.2 Electrospun polymeric nanofibers for tissue engineering

One of the most attractive applications for electrospun polymeric nanofibers is in the tissue engineering field, purposefully for regenerative medicine ^[21]. The nanofibers produced by the electrospinning technique resemble the extracellular matrix (ECM) present in the human body ^[21,22], acting as a scaffold for cell attachment and cell growth (Figure 1.5). The electrospun polymeric scaffolds are good candidates for tissue engineering because they have biomimetic properties, such as fiber diameter with submicron level, large surface to volume ratio, high porosity, variable pore size distribution, and the ability to be tailored into a variety of sizes and shapes ^[20]

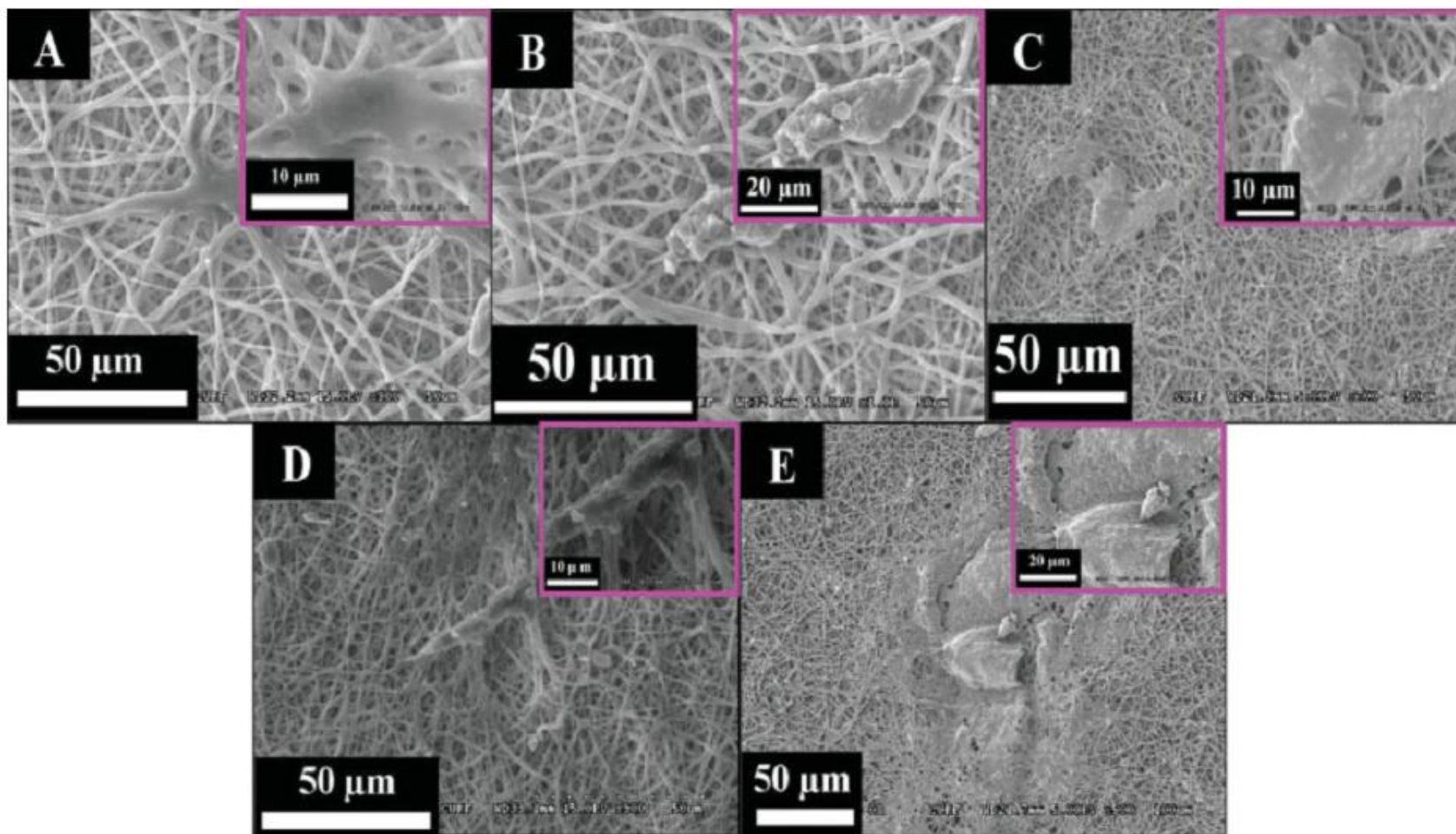


Figure 1.5 SEM images of the nanofiber mats showing cell attachments after 4 days of culturing cells for the prepared silver NPs/PU nanofiber matrices: 0% (A), 2% (B), 5% (C), 7% (D), and 10% (E). The inset in each figure shows high magnification image ^[23].

There are a number of electrospun polymeric nanofibers currently used for tissue engineering applications. The electrospun polymers can be divided into natural and synthetic materials. Examples of natural polymers include collagen, elastin, and silk ^[2,24], which present the advantages of low toxicity and a low chronic inflammatory responses. They can be combined into a composite with other natural or artificial polymers to have improved mechanical properties. However, the disadvantages that natural polymers have are that they often lack sufficient strength and are easily denatured once used out from the natural source ^[25]. To solve the low mechanical strength, they often require chemical modifications, which results in toxicity. Meanwhile, synthetic polymers used to fabricate scaffolds have been investigated in the recent years. Examples of synthetic polymers are poly(glycolic acid) (PGA), poly(lactic acid) (PLA) and their copolymers and poly(ϵ -caprolactone) (PCL) ^[26]. These polymers degrade by hydrolysis of ester bonds and the components are removed by the natural pathways of the body, making them biocompatible and safe for use ^[27].

1.4 Research plan

1.4.1 Project description

The present project involves the synthesis and characterization of polyols, as well as polyurethanes, and fabrication of polyurethane nanofibers. The scope of this research can be followed in three steps. The first step involves synthesizing two different polyols, which are polycaprolactone diol (PCL) and polyvalerolactone diol (PVL). The second step involves synthesizing the polyurethanes based on these two PCL and PVL polyols. Finally, the third step

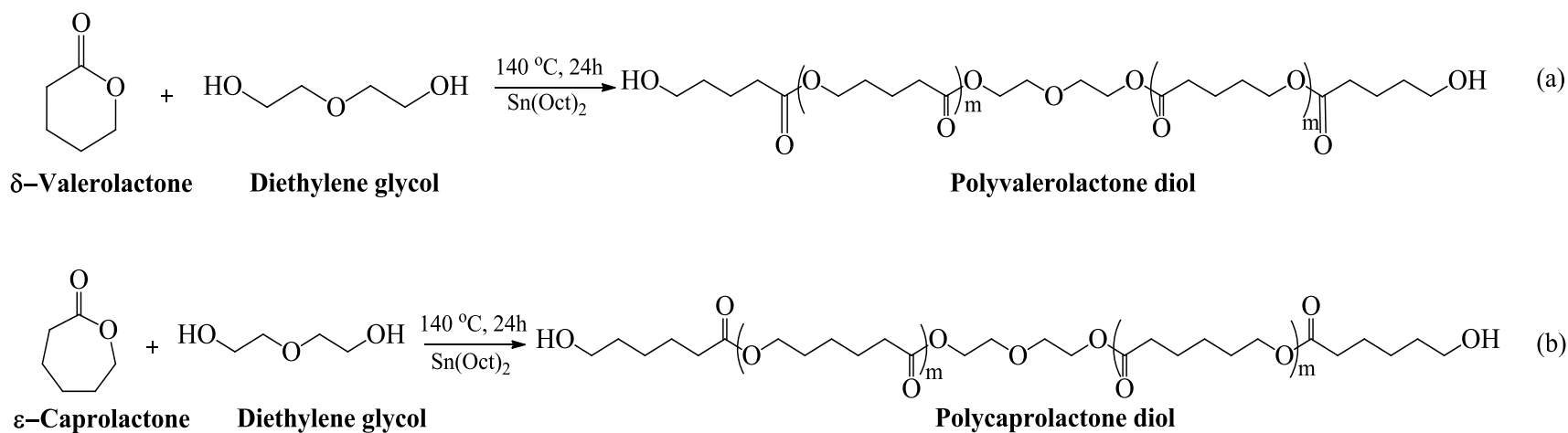
of the project is to electrospin the synthesized polyurethane polymers into nanofibers.

1.4.2 Objectives

The objective of this study is to synthesize, characterize and electrospin biodegradable polyurethane-ureas for biomedical applications.

The synthesis of the polymers will be performed by a two-step method:

- 1) The initial stage will be the synthesis of polycaprolactone diol (PCL) and polyvalerolactone diol (PVL) with different molecular weights using diethylene glycol as an initiator (Scheme 1.5).



Scheme 1.5 Synthesis of polyvalerolactone diol and polycaprolactone diol.

FT-IR, Raman, TGA, DSC and degradability studies.

CHAPTER II
SYNTHESIS OF POLYCAPROLACTONE (PCL), POLYVALEROLACTONE (PVL)
AND CORRESPONDING POLYURETHANES

2.1 Introduction

Polyurethanes have shown great potential and promise in biomedical applications due to their excellent mechanical properties and good biocompatibility. In the past few years, many studies have been done in both non-degradable and biodegradable polyurethanes. However, biodegradable synthetic polyurethanes have a number of advantages over other materials for the fabrication of scaffolds in tissue engineering^[26]. The crucial advantages include the ability to be tailored into a variety of chemical structures, resulting in achievement of different mechanical properties and the ability to degrade in biological environments^[28]. Furthermore, in order to allow cell attachment and growth for applications in tissue engineering, biodegradable synthetic polyurethanes can be designed with chemical functional groups and fabricated into various sizes and shapes with desirable morphologies^[29]. A number of materials have gained tremendous attention for the synthesis of biodegradable polyurethanes. Poly(ϵ -caprolactone) (PCL) and poly(δ -valerolactone) (PVL) are two of the most important and commonly used biodegradable aliphatic polyesters for this purpose^[4]. Both of them can be prepared through ring-opening

polymerization using the cyclic monomer of ϵ -caprolactone (CL) and δ -valerolactone (VL) respectively. PCL is a semi-crystalline polymer having a glass transition temperature of about $-60\text{ }^{\circ}\text{C}$ and melting point ranging between 59 and $64\text{ }^{\circ}\text{C}$. The number average molecular weight of PCL polymers vary from 3000 to $80,000\text{ g/mol}$ ^[30]. This polymer is soluble in chloroform, dichloromethane, carbon tetrachloride, benzene, toluene, cyclohexanone, and 2-nitropropane at room temperature, with low solubility in acetone, 2-butanone, ethyl acetate, dimethylformamide and acetonitrile and is insoluble in alcohol, petroleum ether and diethyl ether ^[30]. PVL is also a biodegradable synthetic polymer that is very attractive due to its properties, such as efficient hydrophobicity and the lack of toxicity and desirable biodegradability. It has a similar structure to PCL, but it has not been used as widely as PCL for biomedical applications ^[6].

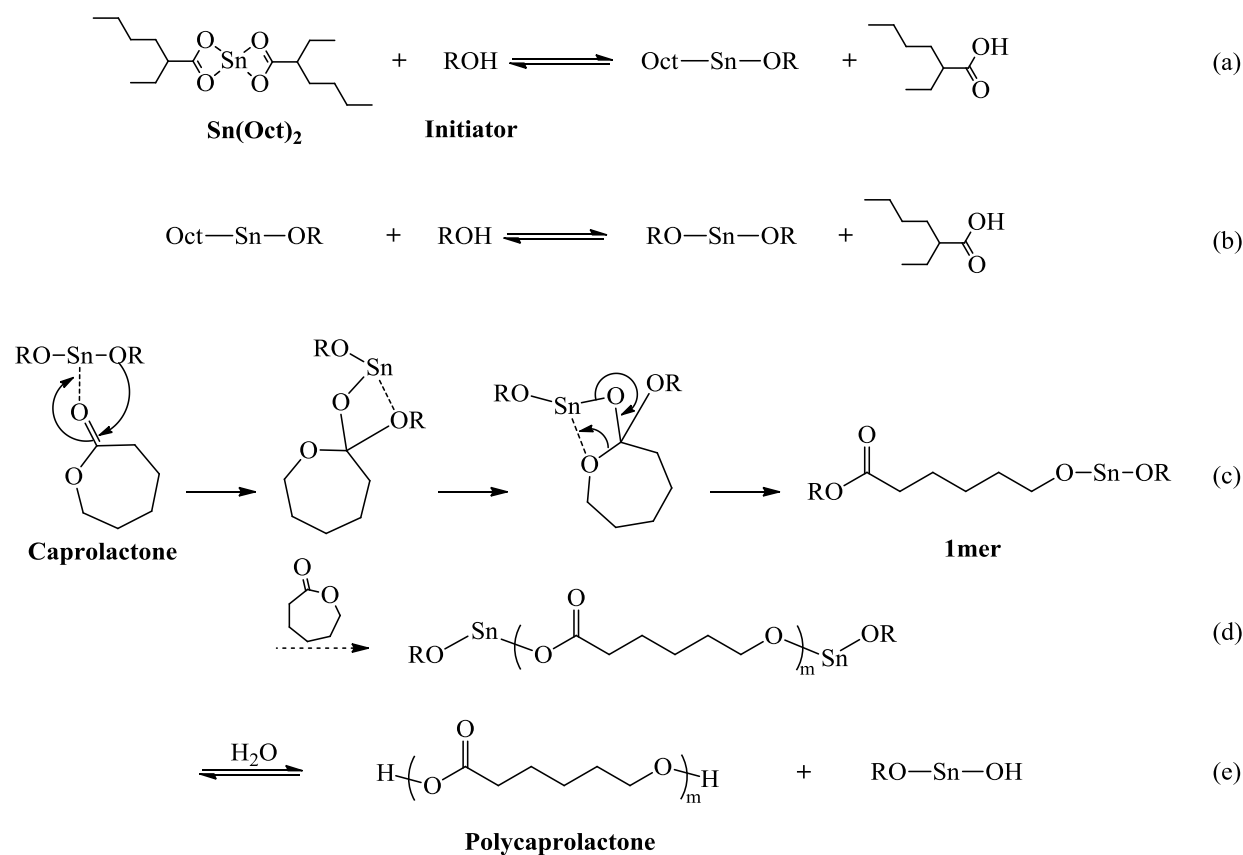
2.2 Materials and Methods

2.2.1 Materials

ϵ -Caprolactone (CL 99%, Acros Organics), δ -valerolactone (VL 99%, Acros Organics), diethylene glycol (DEG reagent, Fisher Chemical), 1,4-diisocyanate butane (BDI, Acros Organics), 1,4-diamino butane (putrescine 99%, Acros Organics), and anhydrous dimethyl sulfoxide (DMSO 99.7%, Extra Dry, Acros Organics) were purified by vacuum distillation before use. Stannous octoate [$\text{Sn}(\text{Oct})_2$, Nusil Technologies], ethanol (Fisher Chemical) and dichloromethane (Fisher Chemical) were used as received.

2.2.2 Synthesis of polyols

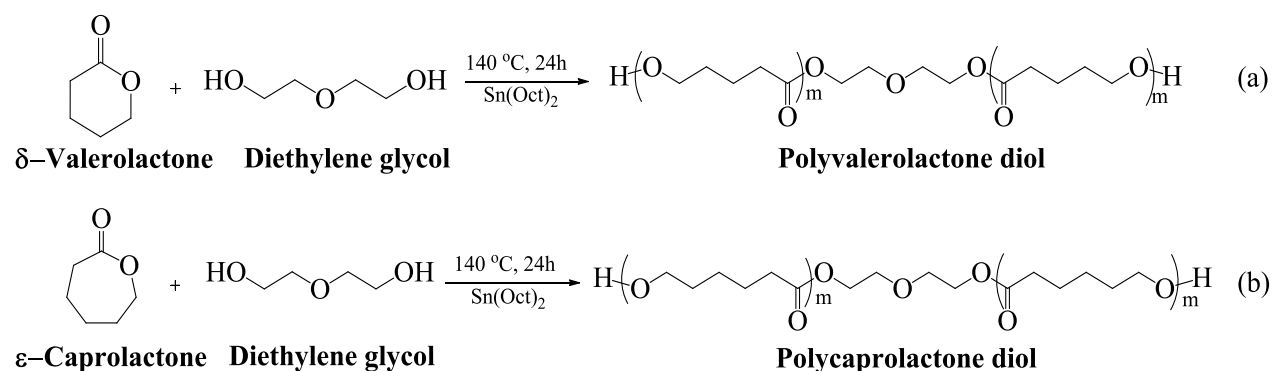
Polycaprolactone diol and polyvalerolactone diol were synthesized by ring-opening polymerization (Scheme 2.1), using Stannous octoate [$\text{Sn}(\text{Oct})_2$] and diethylene glycol (DEG) as a catalyst and an initiator respectively ^[31,32].



Scheme 2.1 Mechanism of Ring-Opening Polymerization of caprolactone under stannous octoate catalyst, (a, b) formation of stannous alkoxide initiator, (c, d) generation of 1mer and polymer, and (e) chain-end deactivation by reacting with water.

In a typical process (Scheme 2.2), the monomer and DEG with variable molar ratios were mixed and heated to 140 °C under argon environment. The catalyst, which is $\text{Sn}(\text{Oct})_2$, was then

added to the solution under stirring conditions at 0.5% wt with respect to the monomer. The reaction was kept for 24 hours to be completed. The obtained products i.e., polycaprolactone diol and polyvalerolactone diol were first cooled down and dissolved in dichloromethane. Then, these products were precipitated in excess of cold ethanol. Finally, the precipitate was filtered and dried under vacuum at room temperature for 3 days.

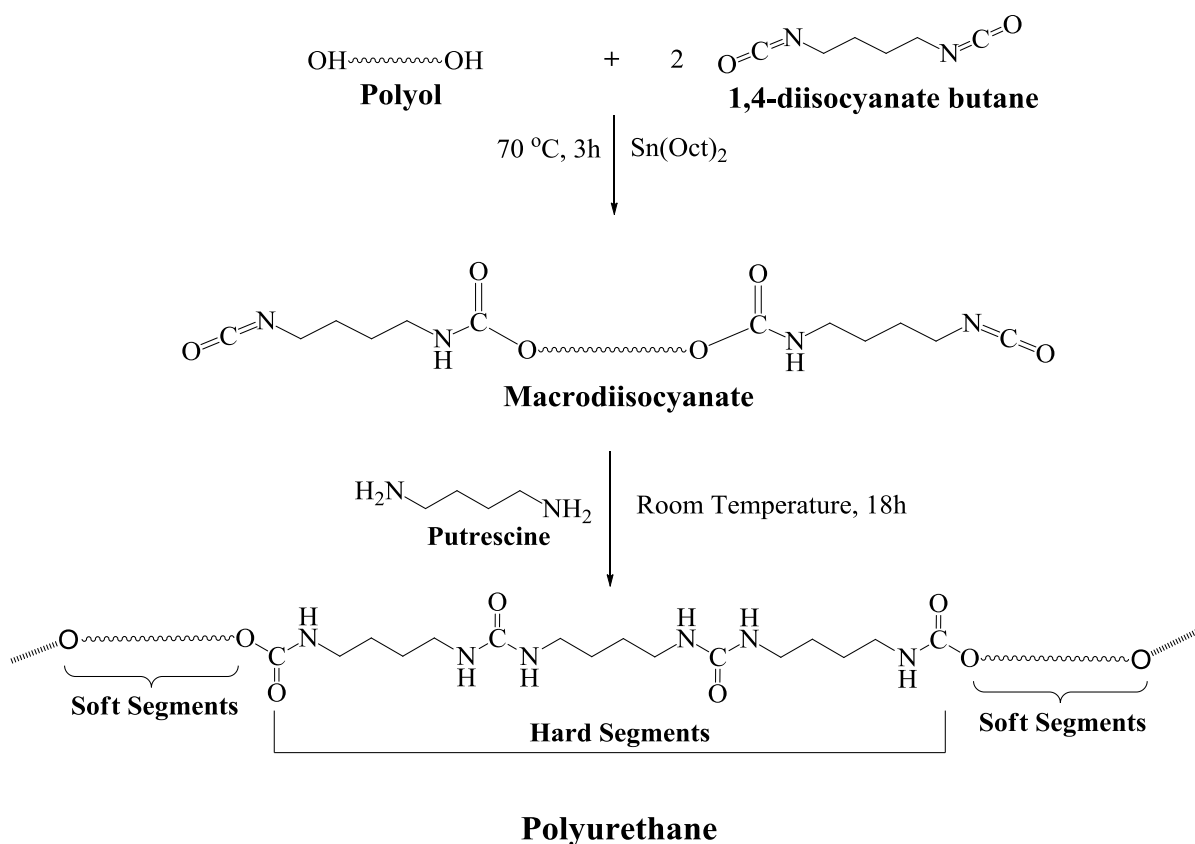


Scheme 2.2 Synthesis of polyvalerolactone (a) and polycaprolactone (b) using diethylene glycol as initiator and stannous octate as catalyst.

2.2.3 Synthesis of polyurethanes

Polyurethanes were synthesized based on polycaprolactone diol and polyvalerolactone diol by a two-step polymerization ^[33] (Scheme 2.3). 1, 4-diamino butane (Putrescine) was used as a chain extender. In a typical process, the synthesis was carried out in a 250-mL three-necked round bottom flask under continuous argon atmosphere. The molar ratio of the reactants was 2:1:1 of BDI: PCL or PVL diol: 1, 4-diaminobutane (putrescine). In the first polymerization step, a 15 wt% solution of BDI in anhydrous DMSO was stirred continuously followed by the addition

of a 25 wt% solution of PCL or PVL diol in anhydrous DMSO. Then, 0.5% wt of $\text{Sn}(\text{Oct})_2$ with respect to the polyols was added. The reaction was allowed to be carried out at 75 °C for a period of 3 hours. In the second step, which is called the chain extension step, the prepolymer solution was cooled down to room temperature, and a putrescine solution in anhydrous DMSO was added to the prepolymer solution in a dropwise manner under vigorous stirring conditions. After that, the reaction was continued at room temperature for 18 hours. The products were precipitated in deionized water. Finally, the obtained polyurethanes were filtered and dried under vacuum at 50 °C for 3 days.



Scheme 2.3 Synthesis of polyurethane by two-step process using BDI and Putrescine.

2.3 Characterizations

2.3.1 Proton Nuclear Magnetic Resonance (^1H NMR)

The chemical structures of caprolactone (CL), valerolactone (VL), diethylene glycol (DEG), 1,4-diisocyanate butane (BDI), 1,4-diamino butane (putrescine), synthesized polycaprolactone diol, polyvalerolactone diol and the polyurethanes were characterized by proton nuclear magnetic resonance method. ^1H NMR spectra of the samples were recorded using a Bruker 600 MHz NMR spectrometer. For each solid sample, around 5 mg of sample were weighed and placed into the NMR tubes followed by the addition of CDCl_3 as a solvent. The scanning number was set at 32. The number average molecular weights of the prepolymers were determined using ^1H NMR spectroscopy by integrating the resonance peak intensity.

2.3.2 Fourier Transform Infrared Spectroscopy (FT-IR)

FT-IR spectra of synthesized samples were collected on a Thermo Nicolet Nexus 470 FT-IR spectrometer equipped with a Nexus DTGS detector at room temperature. The samples used in FT-IR were made in potassium bromide (KBr) pellets. In the case of FT-IR characterization, 1-2 mg of dry samples was weighed and grinded in an agate mortar. Then, 120 mg of dry KBr were added and mixed with samples thoroughly. The scanning numbers were set at 32 under the resolution of 4 cm^{-1} with wavenumbers ranging from $400\text{-}4000\text{ cm}^{-1}$.

2.3.3 Raman spectroscopy

Raman spectra of samples were collected on Bruker Senterra Optic Raman Microscope. The excitation wavelength was set at 785 nm and the laser power to be kept at 50 mW with 50 integrations and 2 co-additions. The spectra were obtained directly from powder samples in the region of 400-3200 cm^{-1} .

2.3.4 Size-exclusive Chromatography (SEC)

Molecular weight M_n and M_w/M_n were determined by size exclusion chromatography (SEC). These analysis were conducted with a Hewlett-Packard instrument (HPLC series 1100) equipped with UV light and refractive index detectors using a series of three PL-Gel columns (10^3 , 10^5 and 10^6 Å) in THF as eluent at 40 °C and at a flow rate of 1 mL/min. The apparent molecular weights (M_n and M_w) were determined with a calibration based on linear polystyrene (PS) standards. Samples were dissolved in THF (1 mg/mL) and inspected to avoid insoluble particles, placed in the appropriated vials before analysis.

2.3.5 Thermogravimetric Analysis (TGA)

Thermogravimetric analysis was used to determine the thermal behavior of the different samples. The experiments were carried out in a TGA 7 (Perkin Elmer). The samples were heated from 20 to 800 °C under nitrogen atmosphere at a flow rate of 20 mL/min. All the scans were started at 20 °C for a minute and then the heating temperature was increased at a rate of 10 °C/min.

2.3.6 Differential Scanning Calorimetry (DSC)

DSC studies were performed using a Perkin Elmer DSC 7 under nitrogen with a flow rate of 20 mL/min. The samples were heated from room temperature to 250 °C for PCL and PVL, room temperature to 300 °C for PU-PCL and PU-PVL using alumina pans. The scanning rates were 10 °C/min.

2.4 Results and Discussions

2.4.1 Synthesis of PCL, PVL, PU-PCL and PU-PVL

Several HO-PCL-OH and HO-PVL-OH polyols with different monomer/initiator ratios were synthesized (Table 2.1). They were prepared by ring-opening polymerization of CL and VL respectively, using Sn(Oct)₂ as a catalyst, and in the presence of DEG as an initiator.

Table 2.1 Synthesis conditions of PCL and PVL polyols.

Polyols	CL or VL : DEG	Sn(oct) ₂	Temperature (°C)	Reaction time (h)
PCL	20:1	0.5% wt	140	24
PVL	20:1	0.5% wt	140	24
PCL	40:1	0.5% wt	140	24
PVL	40:1	0.5% wt	140	24

PU-PCL and PU-PVL were synthesized by reacting the obtained PCL and PVL diols with BDI, followed by a reaction with putrescine. The specific conditions are shown in the Table 2.2.

Table 2.2 Synthesis conditions of PU-PCL and PU-PVL.

Samples	Polyol	BDI	Putrescine	Sn(oct) ₂	Temperature (°C)	Reaction time	Precipitate solvent
	Moles ratio						
	% (w/v) in solvent (DMSO)						
PU-PCL (20:1)	1	2	1	0.5% wt	70-80	3h	Deionized water
	25	15	15		Room Temperature	18h	
PU-PVL (20:1)	1	2	1	0.5% wt	70-80	3h	Deionized water
	25	15	15		Room Temperature	18h	

2.4.2 ^1H NMR

The structures of starting materials (DEG, CL and VL) were determined by ^1H NMR. The typical spectra of those materials were presented in Appendix A.

The chemical structures of synthesized PCL, PVL, PU-PCL and PU-PVL were verified by ^1H NMR spectra. The ^1H NMR spectra of PCL, PVL, PU-PCL and PU-PVL indicate that they were successfully synthesized in our lab.

As for PCL (Figure 2.1), the methylene protons from DEG initiator appeared at $\delta=3.71$ ppm (O-CH_2) and $\delta=4.25$ ppm ($-\text{CH}_2\text{-OCO}$). They were also confirmed by the integrity of the peaks which showed equal intensity. The methylene groups from the monomer CL were assigned to the peaks at $\delta=4.08$ ppm ($\text{O-CH}_2\text{-CH}_2\text{-CH}_2\text{-CH}_2\text{-CH}_2\text{-COO}$), $\delta=2.33$ ppm ($\text{O-CH}_2\text{-CH}_2\text{-CH}_2\text{-CH}_2\text{-CH}_2\text{-COO}$), $\delta=1.66$ ppm ($\text{O-CH}_2\text{-CH}_2\text{-CH}_2\text{-CH}_2\text{-CH}_2\text{-COO}$), and $\delta=1.40$ ppm ($\text{O-CH}_2\text{-CH}_2\text{-CH}_2\text{-CH}_2\text{-CH}_2\text{-COO}$) respectively. The chemical shift at $\delta=3.67$ ppm ($\text{HO-CH}_2\text{-CH}_2\text{-CH}_2\text{-CH}_2\text{-CH}_2\text{-COO}$) was attributed to the methylene group next to the terminated hydroxyl group in PCL. This was further verified by the absence of the peak in ^1H NMR spectrum of PU-PCL.

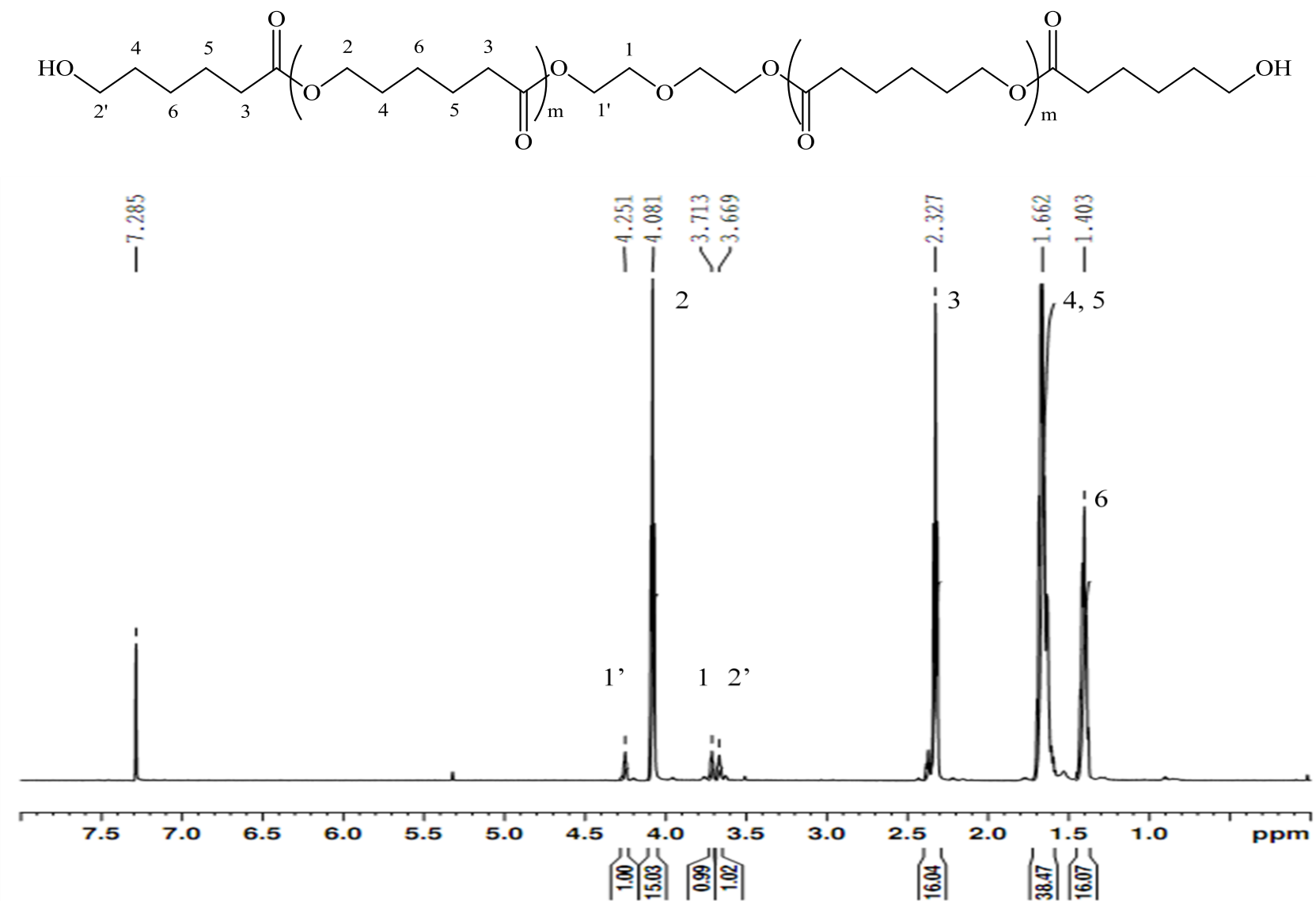


Figure 2.1 ^1H NMR spectrum of synthesized PCL 20:1.

A typical ^1H NMR spectrum of PVL (Figure 2.2) was also observed that shows the similar chemical shifts of peaks to those of PCL. The methylene groups from the monomer VL were assigned to the peaks at $\delta=4.10$ ppm ($\text{O-CH}_2\text{-CH}_2\text{-CH}_2\text{-CH}_2\text{-COO}$), $\delta=2.36$ ppm ($\text{O-CH}_2\text{-CH}_2\text{-CH}_2\text{-CH}_2\text{-COO}$), $\delta=1.70$ ppm ($\text{O-CH}_2\text{-CH}_2\text{-CH}_2\text{-CH}_2\text{-COO}$), and $\delta=3.67$ ppm ($\text{HO-CH}_2\text{-CH}_2\text{-CH}_2\text{-CH}_2\text{-COO}$) respectively. The chemical shifts of methylene groups from DEG in PVL were consistent with that in PCL, which were at $\delta=3.71$ ppm (O-CH_2) and $\delta=4.25$ ppm ($\text{-CH}_2\text{-OCO}$).

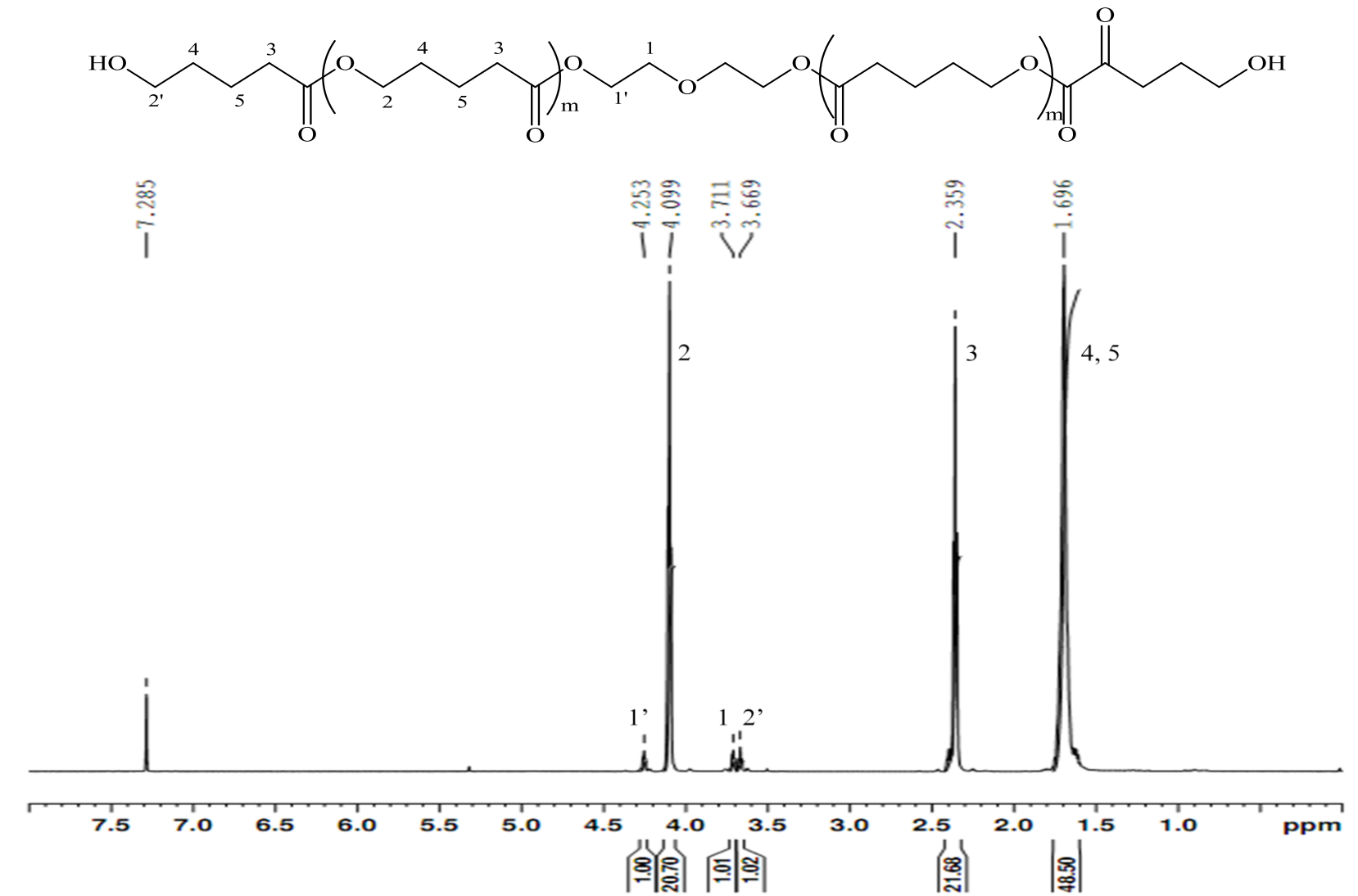


Figure 2.2 ^1H NMR spectrum of synthesized PVL 20:1.

The putrescine and BDI for synthesis of polyurethanes were also verified by ^1H NMR spectroscopy. In this regard, the Appendix A shows the spectra obtained from ^1H NMR data.

In case of polyurethanes, ^1H NMR showed that the syntheses were completed in a successful manner (Figure 2.3). In the ^1H NMR spectra of PU-PCL, as indicated in this figure, the peaks at $\delta=4.25$, 4.08, 3.72, 2.33, 1.40 ppm are corresponding to the soft segments of PCL chains. The additional peak at $\delta=3.21$ ppm ($-\text{CH}_2\text{-NH}-$), comparing from spectrum of PCL, can be assigned to methylene group from hard segments. The chemical shifts of other methylene group from hard segments at $\delta=1.66$ ppm ($-\text{CH}_2\text{-CH}_2\text{-CH}_2\text{-CH}_2-$) were mixed with those from soft segments of PCL. The absence of peaks at $\delta=3.67$ ppm indicated that the PCL polyol had completely reacted with diisocyanate, resulting in the formation of prepolymer.

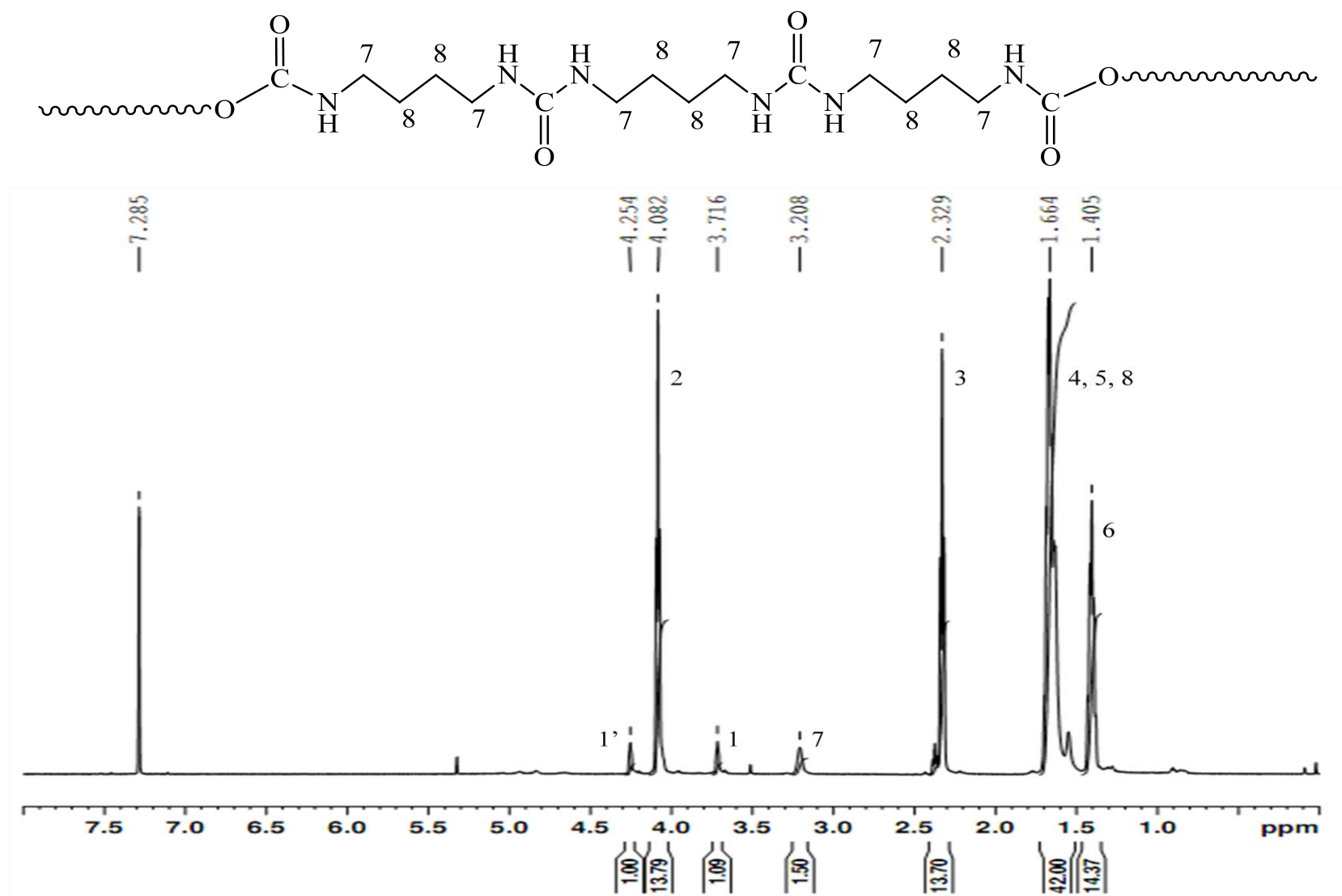


Figure 2.3 ^1H NMR spectrum of synthesized PU-PCL 20:1.

The number-average molecular weight (M_n) of polyols PCL and PVL and polyurethanes were determined with their ^1H NMR spectra through the ratios between integrals of peak characteristic of the main chain and those of the chain terminals ending with hydroxyl groups. As an example of PCL, the integral ratio can be obtained from the mole ratio of the CL repeating unit and the DEG component by using the equation: $R = (I_3/2) / (I_1/4) = 2I_3 / I_1$, where I_1 and I_3 stand for the integrations of methylene proton of DEG component (with 4H atoms) and methylene proton of CL component (with 2H atoms) respectively. The number-average molecular weight of PCL can be calculated by adding the molecular weight of each component, and the molecular weight of each component is obtained by multiplying the mole number by the relative molecular weight ^[34]. The number-average of molecular weights of all synthesized polyols are shown in Table 2.3.

Table 2.3 Number-average of molecular weights of synthesized polyols.

Samples	M_n (g/mol)
PCL (20:1)	3,754
PCL (40:1)	4,215
PVL (20:1)	4,406
PVL (40:1)	3,310

2.4.3 FT-IR

FT-IR spectra together with ^1H NMR spectra indicate that the polycaprolactone, polyvalerolactone and polyurethane were successfully synthesized. Typical FT-IR spectra of PCL

and PU-PCL are shown in Figure 2.4.

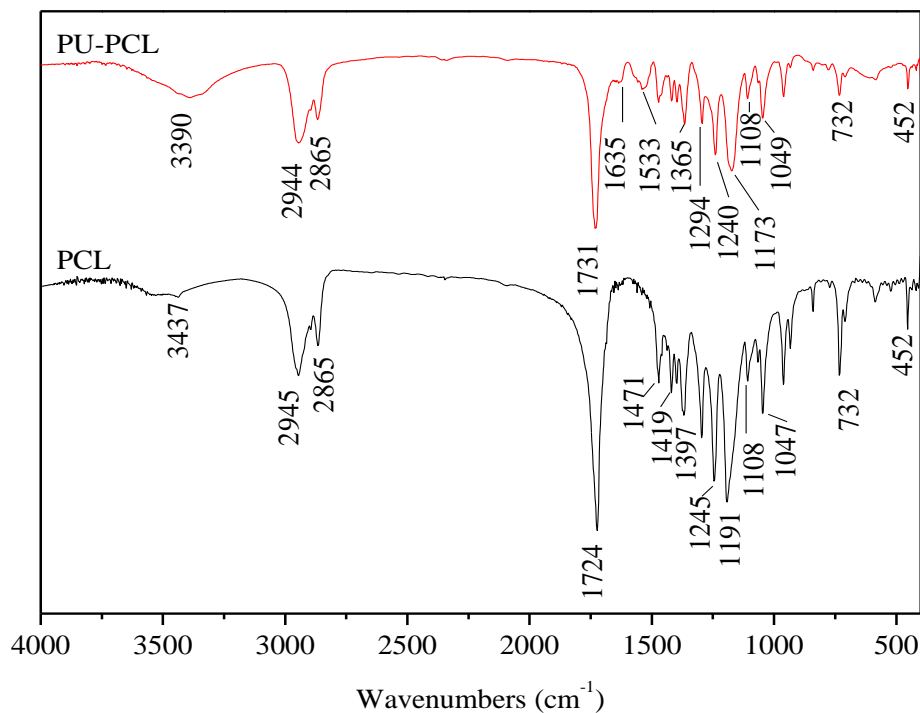


Figure 2.4 FTIR spectra of synthesized PCL and PU-PCL.

Asymmetric and symmetric CH₂ stretching vibration peaks of the PCL soft segments are located at 2944 and 2865 cm⁻¹, respectively. Other modes of CH₂ vibrations are characterized by the bands at 1471, 1419, 1397, 1365, 1294 and 732 cm⁻¹. Comparison with the spectra of PCL polyols, the presence of characteristic polyurethane bands are confirmed with the bands in the region of 3150-3500 cm⁻¹ and 1500-1800 cm⁻¹ [35]. The bands at 3150-3500 cm⁻¹ are assigned to NH stretching vibrations from urethane and urea groups in the hard segments of polyurethanes. The absorption of amide I is located in the range 1600-1800 cm⁻¹ including C=O stretching vibrations at 1731 cm⁻¹ and C-N stretching at 1635 cm⁻¹ [15]. The peaks at 1500-1600 cm⁻¹ are attributed to amide II, which are N-H bending, C-N stretching and C-C stretching vibrations.

Characteristic absorbance for the soft segments at 1240 cm^{-1} and 1047 cm^{-1} are attributed to C-O-C asymmetric and symmetric stretching, respectively, while C-O-C bending vibrations appeared at 452 cm^{-1} . The bands at 1173 and 1108 cm^{-1} are assigned to O=C-O ester group in both soft and hard segments ^[34,35]. Characteristic peaks assignments of PCL and PU-PCL were listed in Table 2.4 and Table 2.5.

Table 2.4 Characteristic FT-IR peaks assignments of PCL.

Frequency (cm^{-1})	Assignments	Abbreviation
3437	OH stretching	ν (OH)
2944	Asymmetric stretching	ν_{as} (CH_2)
2865	Symmetric stretching	ν_{s} (CH_2)
1724	Carbonyl stretching	ν (C=O)
1471, 1419, 1398, 1369	CH_2 bending, CH_2 wagging	δ (CH_2), ω (CH_2)
1295	C-O and C-C stretching in the crystalline phase	ν_{cr}
1245	Asymmetric COC stretching	ν_{as} (COC)
1191	OC-O stretching	ν (OC-O)
1108	OC-O stretching ester bonds	ν (OC-O)
1047	-C-O-C- in the ether segment	ν (-C-O-C-)

Table 2.5 Characteristic FT-IR peaks assignments of PU-PCL.

Frequency (cm ⁻¹)	Assignments	Abbreviation
3330-3450	N-H stretching	ν_s (N-H)
2944	Asymmetric stretching	ν_{as} (CH ₂)
2865	Symmetric stretching	ν_s (CH ₂)
1731	Carbonyl stretching	ν (C=O)
1635	Amide I	ν (C-N)
1533	Amide II	δ (N-H), ν (C-N)
1472, 1419, 1397, 1365	CH ₂ bending, CH ₂ wagging	δ (CH ₂), ω (CH ₂)
1294	C-O and C-C stretching in the crystalline phase	ν_{cr}
1240	Asymmetric COC stretching	ν_{as} (COC)
1173, 1108	OC-O stretching ester bond	ν (OC-O)
1108	OC-O stretching ester bond	ν (OC-O)
1049	-C-O-C- in the ether segment	ν (-C-O-C-)

FT-IR spectra of synthesized PVL and PU-PVL were obtained in Figure 2.5. Asymmetric CH₂ stretching vibration peaks of the PVL are located at 2959 cm⁻¹. However, the symmetric CH₂ stretching vibration shows a doublet at 2894 and 2875 cm⁻¹. Other modes of CH₂ vibrations are characterized by the bands at 1475, 1425, 1397, 1326, 1259 and 740 cm⁻¹. Comparison with the spectra of PVL polyols, the presence of broad bands at 3150-3500 cm⁻¹ are assigned to NH stretching vibrations from urethane and urea groups in the hard segments of polyurethanes. The C=O stretching vibrations were observed at 1732 cm⁻¹ and C-N stretching at 1624 cm⁻¹ [15]. The peaks at 1541 cm⁻¹ are attributed to amide II, which are N-H bending, C-N stretching and C-C

stretching vibrations. Characteristic absorbance for the soft segments at 1257 cm^{-1} and 1045 cm^{-1} are attributed to C-O-C asymmetric and symmetric stretching, respectively, The bands at 1173 and 1108 cm^{-1} are assigned to O=C-O ester group in both soft and hard segments ^[34,35].

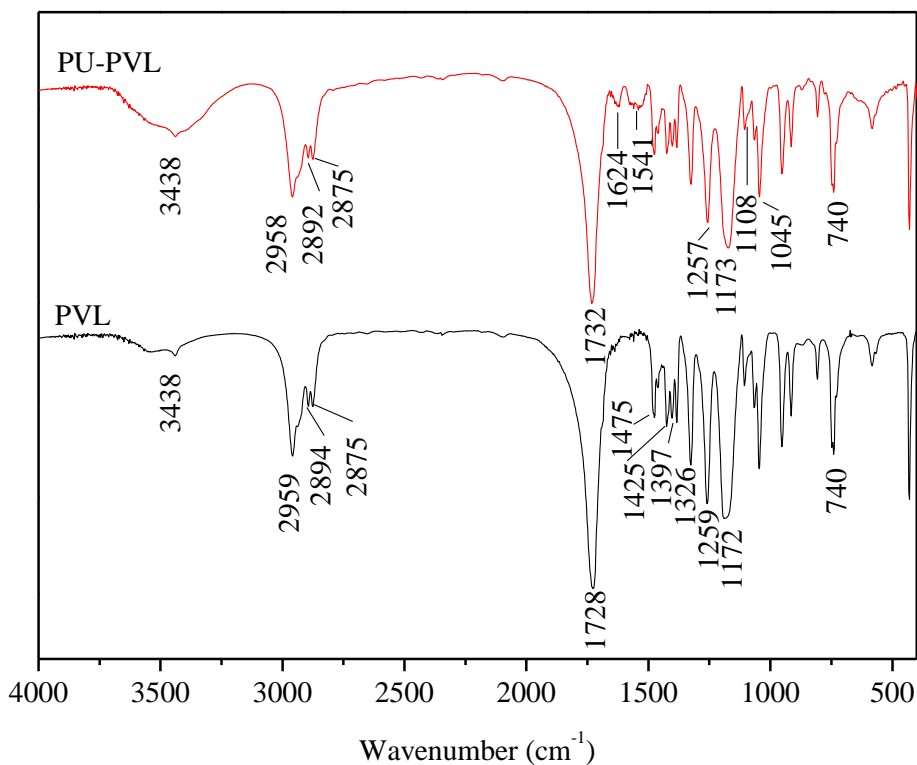


Figure 2.5 FTIR spectra of synthesized PVL and PU-PVL.

2.4.4 Raman

Due to the instrumental limitation, the Raman spectra were obtained in the range of only 80 to 3200 cm^{-1} . Figure 2.6 shows the Raman spectra of starting materials, which are diethylene glycol, putrescine and BDI. The spectra are typical due to the presence of characteristic peaks for each reagent used in these experiments. In the case of DEG, the bands are observed at 2938 and

2871 cm^{-1} (asymmetric and symmetric CH_2 stretching), 1457 cm^{-1} (CH_2 scissoring), 1278 cm^{-1} (CH_2 wagging), and 1082 cm^{-1} (skeletal vibration), respectively. The peaks at 822 cm^{-1} and 896 cm^{-1} are assigned to stretching vibration of C-O-C group in the DEG. The Raman spectrum of putrescine shows the main characteristic vibrations of CH_2 groups. Raman spectrum for BDI indicates the similar characteristic CH_2 group vibrations are present. However, the vibration of functional group corresponding to $\text{N}=\text{C}=\text{O}$ are slightly shown in the region of 2230 cm^{-1} [38].

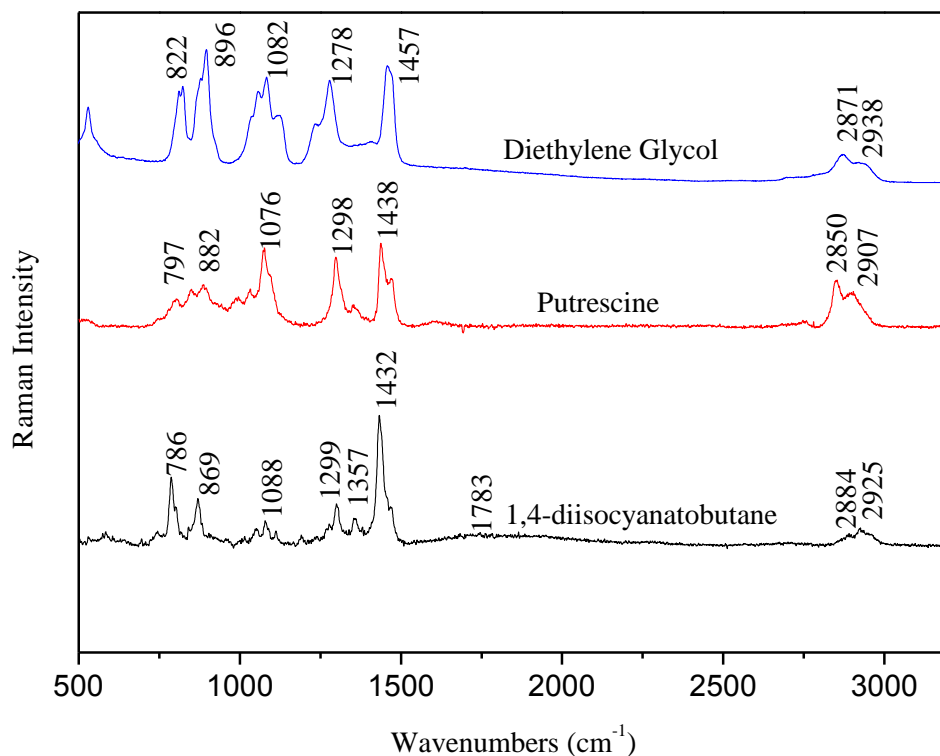


Figure 2.6 Raman spectra of diethylene glycol, putrescine, and 1,4-diisocyanate (BDI).

Figure 2.6 shows the Raman spectra of commercial CL monomer, and synthesized PCL and PU-PCL polymers. As seen in Figure 2.6, Raman spectra of CL and PCL confirmed the IR

findings. Polycaprolactone was successfully synthesized, as confirmed by the significant decrease in intensity of peaks at 696 cm^{-1} and 734 cm^{-1} , which are assigned to the asymmetric and symmetric ring-stretching from CL. The very weak peaks found at 696 cm^{-1} and 734 cm^{-1} from PCL could be attributed to the non-reacted CL. In addition, bands at 848 cm^{-1} belonging to stretching vibration of C-O-C(O) shifted to higher frequency in the spectrum of PCL^[39].

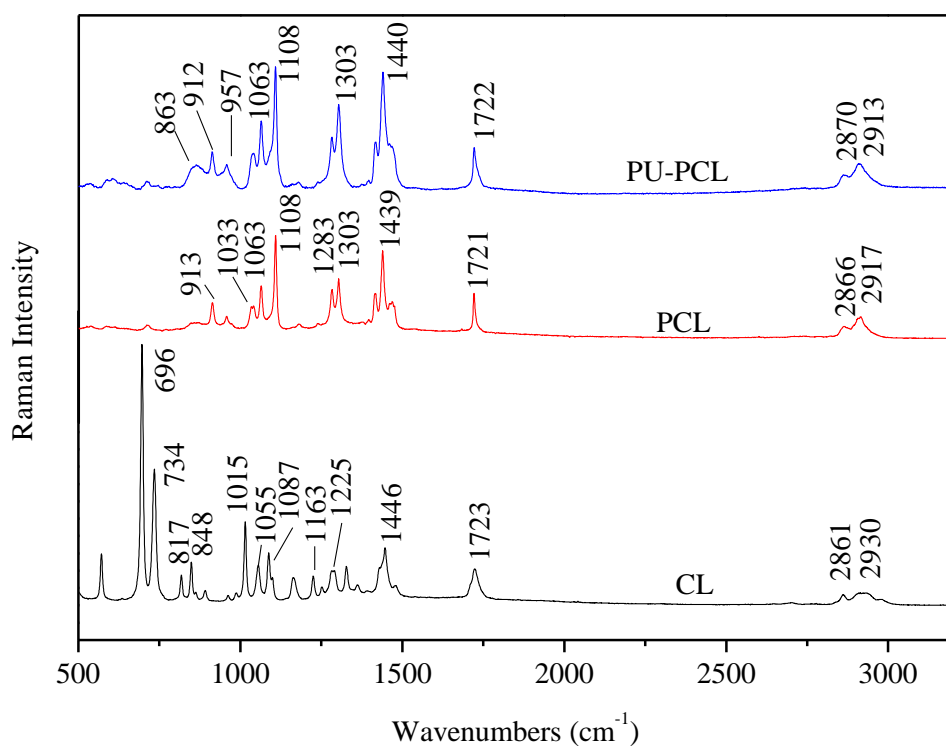


Figure 2.7 Raman spectra of CL, PCL and PU-PCL.

The peak at 1721 cm^{-1} , corresponding to C=O stretching vibration, became sharper and slightly shifted comparing with that of CL. Furthermore, there is no dramatic difference between the spectra of PCL and that of PU-PCL. It is observed that the intensity of peaks at 912 cm^{-1}

increased ^[40]. The peaks assignment of CL and PCL are also listed in Table 2.6.

Table 2.6 Characteristic peaks assignment for CL and PCL.

CL		PCL	
Frequency (cm ⁻¹)	Assignments	Frequency (cm ⁻¹)	Assignments
2930	Asymmetric CH ₂ stretching	2917	Asymmetric CH ₂ stretching
2861	Symmetric CH ₂ stretching	2866	Symmetric CH ₂ stretching
1723	Carbonyl stretching	1721	Carbonyl stretching
1469, 1439, 1417	CH ₂ bending	1469, 1439, 1417	CH ₂ bending
1303, 1283	CH ₂ wagging	1303, 1283	CH ₂ wagging
696	Asymmetric ring-stretching	1108, 1063	Skeletal vibration

Similar Raman results for PVL and PU-PVL were shown in Figure 2.8. The peaks at 748 cm⁻¹, which are assigned to the asymmetric and symmetric ring-stretching from VL, had mostly disappeared in the spectra of PVL. It indicates that the PVL had been successfully synthesized. The presence of tiny peaks found at 748 cm⁻¹ could be attributed to the non-reacted VL monomers ^[39]. In addition, the bands at around 929 cm⁻¹ belonging to stretching vibration of C-O-C(O) had been observed an increase in intensity in the spectrum of PVL. The C=O stretching vibration at 1721 cm⁻¹ became sharper and slightly shifted comparing with that of VL. Furthermore, no dramatic difference between the spectra of PVL and that of PU-PVL was shown.

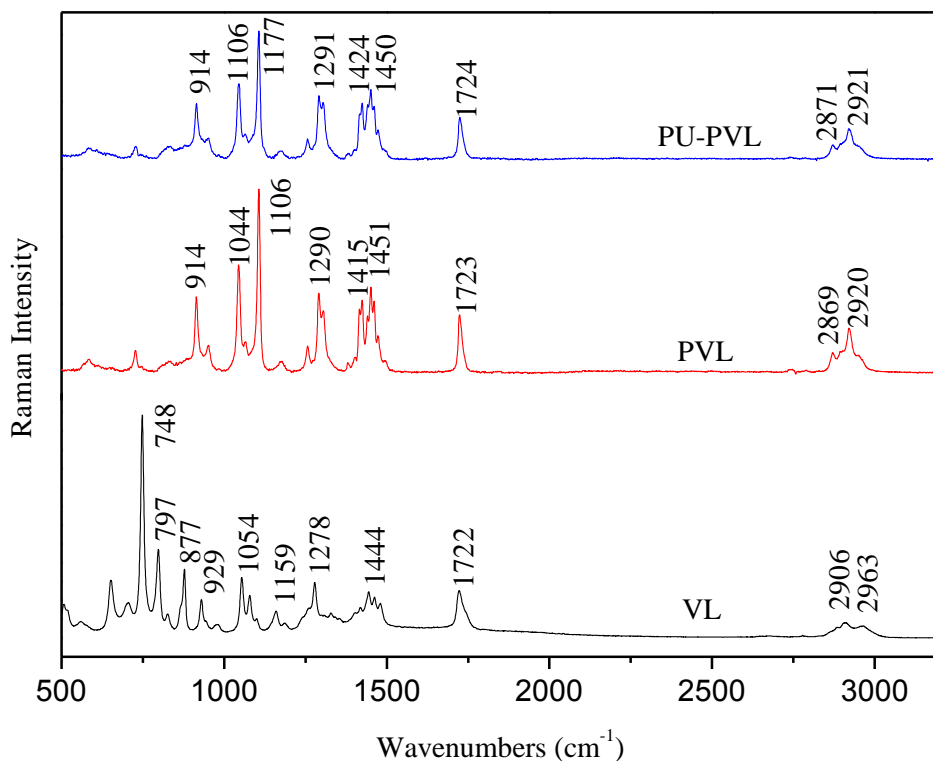


Figure 2.8 Raman spectra of VL, PVL and PU-PVL

2.4.5 SEC

The molecular weight data (M_n) and polydispersity index (M_w/M_n) of synthesized PCL, PVL and PU-PVL are present in Table 2.7. The M_n evaluated by ^1H NMR and those measured by SEC were in good agreement. As SEC data indicate, the obtained PCL polyol had a 5,000 g/mol molecular weight as well as PVL. It is observed that the molecular weight of PCL polyol increases by 1,000 g/mol with the increase in ratio of CL/DEG (monomer to initiator ratio). However, as VL/DEG ratio was increased from 20:1 to 40:1, the molecular weights decreased by 1,600 g/mol, which were much lower than the calculated one from that all monomers were

converted into polymer chains. It suggested that the reaction mixture could be in equilibrium between polymerization and depolymerization after enough reaction time at high temperature ^[41].

Table 2.7 SEC results of synthesized polyols and polyurethanes.

Samples	M_n^a	M_n^b	M_w/M_n^c	M_p^d
PCL (20:1)	3,754	4,844	1.47	5,806
PCL (40:1)	4,215	5,827	1.48	8,330
PVL (20:1)	4,406	5,868	1.36	7,862
PVL (40:1)	3,310	4,218	1.47	5,560
PU-PCL (20:1)	-	Insoluble	Insoluble	Insoluble
PU-PVL (20:1)	-	12,637	2.27	21,275

^a Determined by ¹H NMR. (M_n = number-average molecular weight)

^b Determined by SEC. (M_w = weight-average molecular weight)

^c Determined by SEC. (M_w/M_n = PDI, also known as polydispersity)

^d Determined by SEC. (M_p = molecular weight of the highest peak)

It was reported by Vivas and coworkers that as δ -valerolactone polymerized with diphenylzinc, the molecular weight of the resulting polymers decreased when the temperature was over 60°C, suggesting that ‘back-biting’ of the active chain-end causes decomposition and formation of oligomers and consequently may cause a decrease of molecular weight ^[42,43]. Furthermore, the structures of cyclic ester is another important factor in the ring-opening polymerization of δ -valerolactone and ϵ -caprolactone ^[44]. Saiyasombat and coworkers studied the ring strain and polymerizability of cyclic esters. It was concluded that as the ring size

increases from 5 to 7 (γ -butyrolactone, δ -valerolactone and ϵ -caprolactone), the ring strain also increases. In the case of polymerizability, the larger cyclic monomers can be more easily polymerized^[43,44]. The polydispersity index, with the increase of monomer to initiator ratio, two different PCLs had a constant molecular weight distribution (1.47 and 1.48). Nevertheless, it was found that there was a slightly change in PDI values of PVLs (1.36 and 1.47). The SEC traces curves of four polyols were illustrated in Figure 2.9. It depicts that all peaks were single bell-shaped and no other small peaks indicating that the monomer and initiator were all consumed to get the final polyol products.

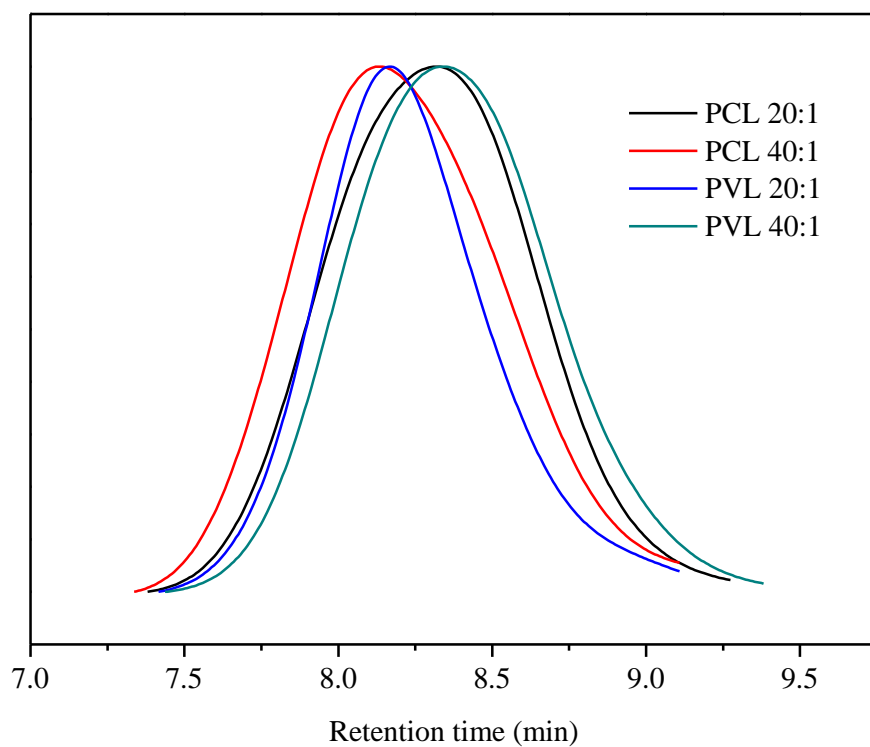


Figure 2.9 Overlay of SEC curves for PCL (20:1 and 40:1) and PVL (20:1 and 40:1).

Molecular weight of synthesized polyurethanes with varying soft segments, which are PCL and PVL, were also determined by SEC. As can be seen in Table 2.7, polyurethane based on PCL 20:1, did not dissolve in the THF eluent. The insolubility of PU-PCL 20:1 indicates that a relatively high molecular weight was obtained during synthesis. In the case of PU-PVL 20:1, the SEC analysis implied a 12,637 g/mol molecular weight with a high molecular weight fraction of (2.27). Furthermore, the SEC trace curve shown in Figure 2.10 was a broad peak with another small peak. It can be taken into account that PVL was not totally consumed or reacted resulting in the lower molecular weights. It is also confirmed with the result from ^1H NMR and FTIR characterizations.

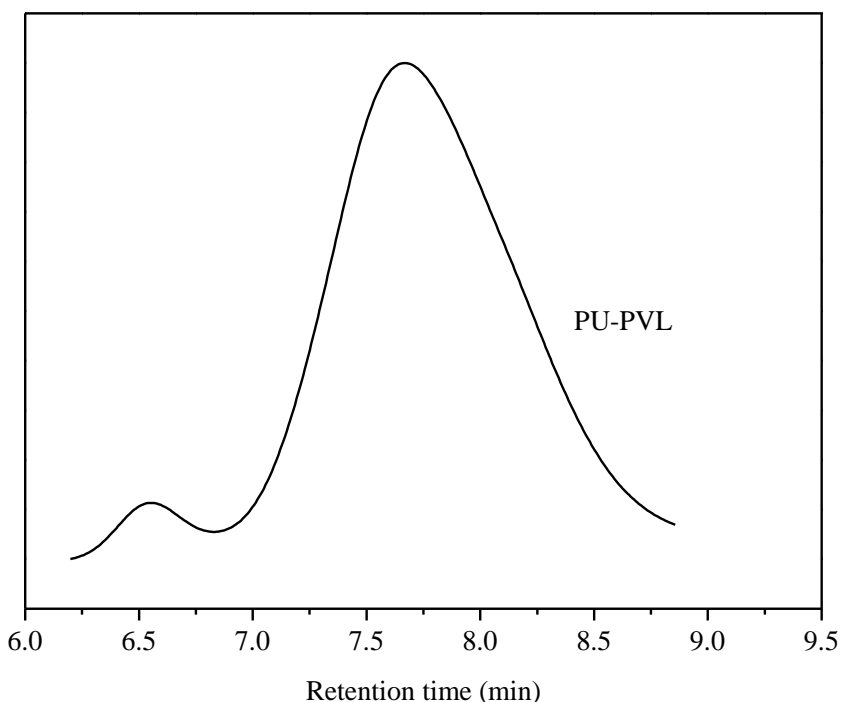


Figure 2.10 SEC curves of polyurethane prepared from PVL 20:1.

2.4.6 TGA

The thermal stability of synthesized PCL, PVL, PU-PCL, and PU-PVL were evaluated using TGA. Onset temperatures of all samples are listed in Table 2.8. The TGA results show that the thermal properties of samples are correlative of the molecular weights of samples, confirmed with the SEC results. With increased molecular weights, the onset temperature of PCL 40:1 is 10 °C higher than that of PCL 20:1. In contrast, the onset temperature of PVL 40:1 is decreased by 22 °C with comparison of that of PVL 20:1. On the other hand, the onset temperatures of the corresponding polyurethanes are higher than those of PCL and PVL, which are 28 °C and 7 °C. It's also in agreement with SEC results.

Table 2.8 Onset decomposition temperatures for PCL, PU-PCL, PVL and PU-PVL.

Samples	Onset decomposition temperature (°C)
PCL 20:1	309
PCL 40:1	319
PU-PCL20:1	337
PVL 20:1	293
PVL 40:1	267
PU-PVL 20:1	300

Figure 2.11 shows TGA results for PU-PCL polymer compared with the PCL. Both, the obtained PCL 20:1 and PCL 40:1 implied single-step decomposition profiles showing a sharp

drop. The PCL 40:1 indicated higher thermal stability than that of PCL 20:1 because it started to lose weight at ~248 °C ending degradation at ~411 °C, whereas the PCL 40:1 started degrading at ~225 °C and completed at ~347 °C^[45].

Furthermore, the onset temperature is 309 °C for PCL 20:1 and 319 °C for PCL 40:1, respectively. In comparison with PCL 20:1, the PCL 40:1 has 10 °C higher onset that is attributed to the relative high molecular weight of PCL 40:1. Similar weight loss curve was observed for the polyurethane based on PCL 20:1. The degradation of PU-PCL 20:1 started approximately at ~257 °C and was completed at ~412 °C. The onset temperature of PU-PCL 20:1 was shown at 337 °C. It is obvious that PU-PCL 20:1 is much more thermally stable than PCL 20:1.

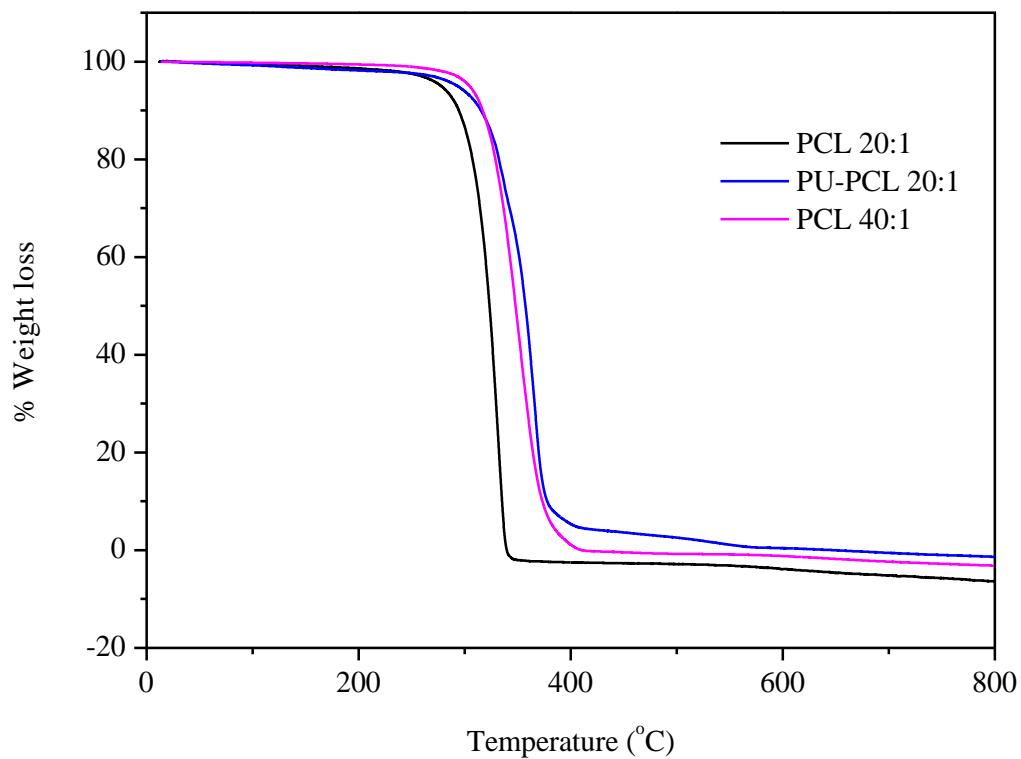


Figure 2.11 TGA curves of PCL (20:1 and 40:1) and PU-PCL 20:1.

As can be seen from Figure 2.12, similar TGA curves were plotted and obtained for PVL, PU-PVL. Due to the low molecular weight of PVL 40:1 comparing to that of PVL 20:1, the decomposition temperature for PVL 40:1 is 267 °C, indicating that it is approximately 30 °C lower than PVL 20:1 (293 °C). Furthermore, the degradation of PVL 40:1 began at 193 °C and was completed at 330 °C, while PVL 20:1 started at 187 °C and ended at 350 °C. It is also clear that the PU-PVL 20:1 had a better thermal stability than PVL 20:1 [46].

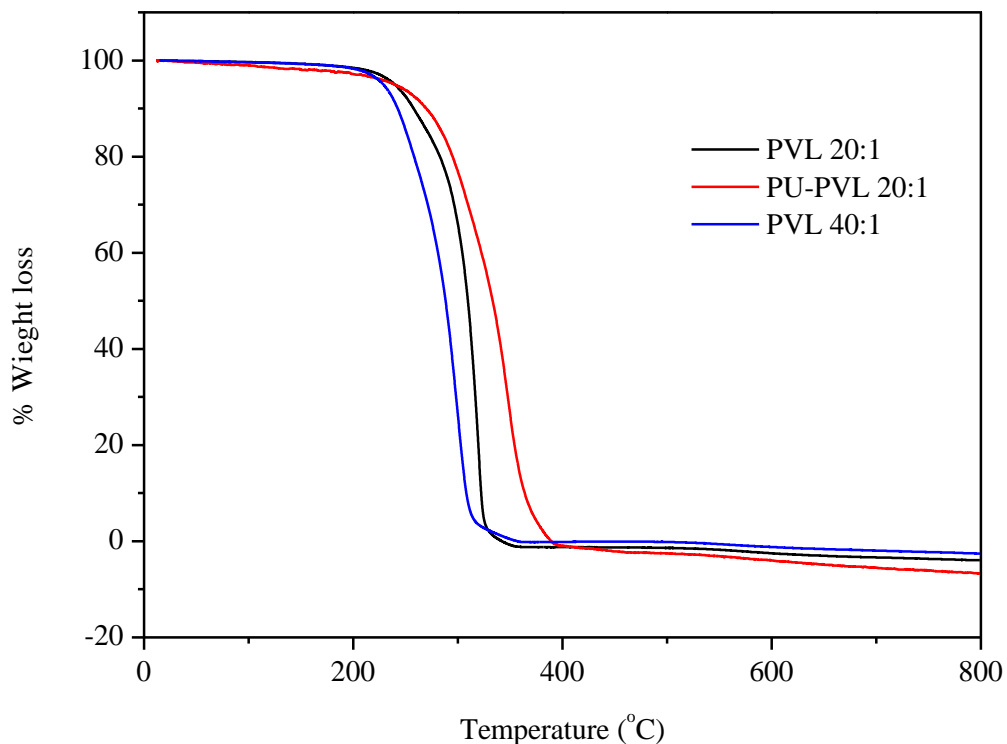


Figure 2.12 TGA curves of PVL (20:1 and 40:1) and PU-PVL 20:1.

2.4.7 DSC

Figure 2.13 shows DSC thermograms of PCL and PU-PCL in first heating, first cooling and second heating, respectively. All melting temperatures of samples (T_m) determined by DSC are listed in Table 2.9. For all samples, the glass transition temperatures (T_g) were not able to be measured due to the out range of temperature in the instrument used.

Figure 2.13a shows the obtained DSC data of PCL20:1; it is found that there is a double endothermic behavior for melting during the first heating cycle. This indicates the presence of two distinct crystalline zones in PCL20:1, which could be attributed to different degrees of

ordering or size in the crystallites ^[47]. In the second heating, the melting peaks shifted to lower temperatures with a decrease in the intensity of higher melting peak and an increase in that of lower melting peak. Nevertheless, the subsequent melting cycles do not seem to alter the crystalline features of polyols ^[47]. For PCL 40:1 (Figure 2.13b), the endotherms remained the same thermal behavior, except for the broad single peak in the first running.

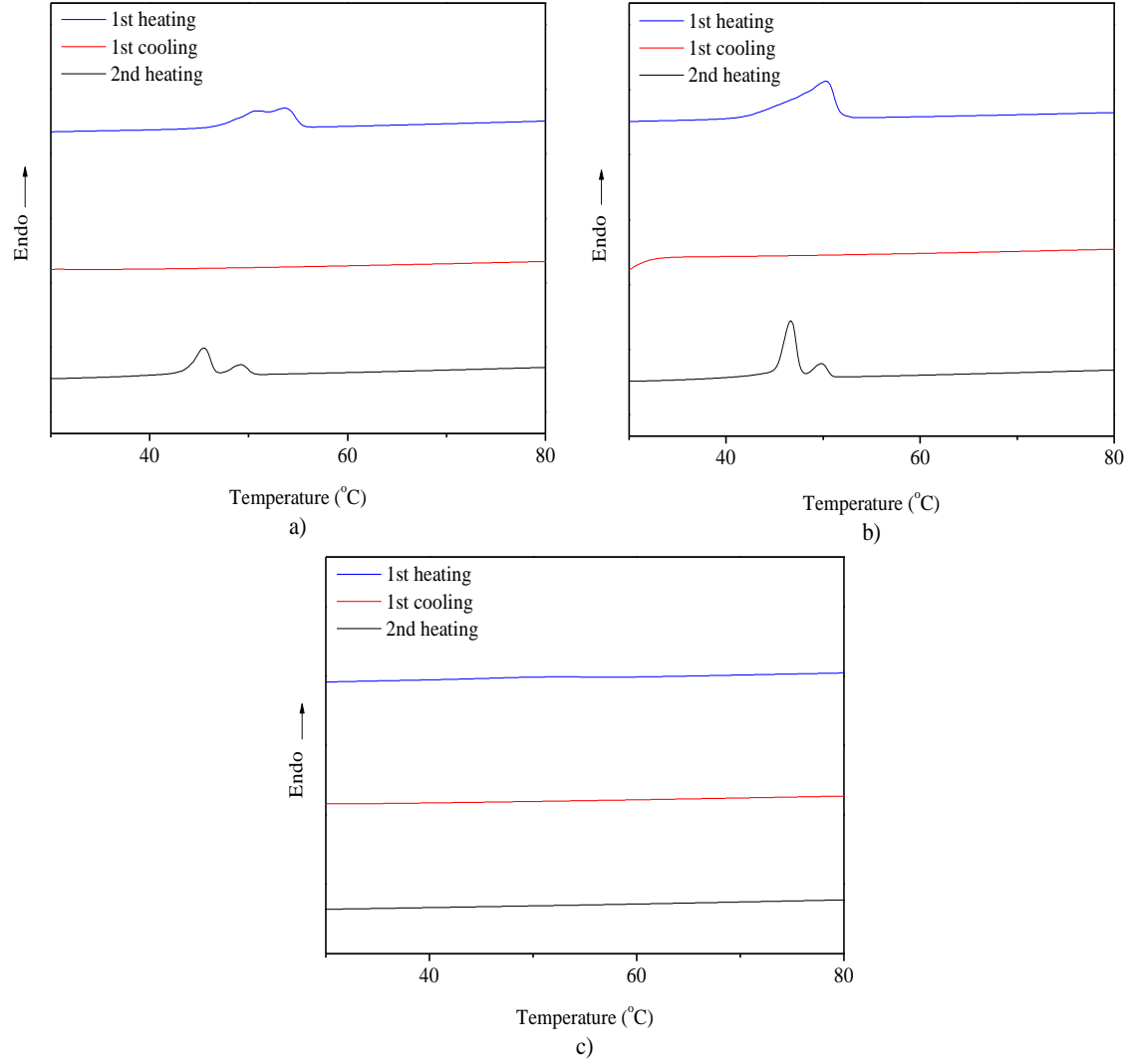


Figure 2.13 DSC of (a) PCL 20:1, (b) PCL 40:1, (c) PU-PCL 20:1.

Table 2.9 DSC data of PCL, PU-PCL, PVL and PU-PVL.

Samples	T_m (°C)	
	1 st heating	2 nd heating
PCL 20:1	50, 53	45, 49
PCL 40:1	50	47, 50
PU-PCL 20:1	49, 53	-
PVL 20:1	50	45
PVL 40:1	47	42
PU-PVL 20:1	55, 59	-

The DSC curves of polyurethane derived from PCL 20:1 were shown in Figure 2.13c. The melting temperature of the polymer was the same as that of the pure PCL 20:1. After first heating, the polymer did not retain its crystallinity because of the absence of melting peak recorded in the second heating.

In Figure 2.14, DSC results of PVL 20:1 represented a melting temperature of 50 °C, whereas PVL 40:1 was determined at 47 °C. The obtained PVL only showed a single endothermic peak suggesting that only one crystalline zone existed in each sample. For the polyurethane derived from PVL 20:1, it started melting at 55 and 59 °C with a double endotherm peak.

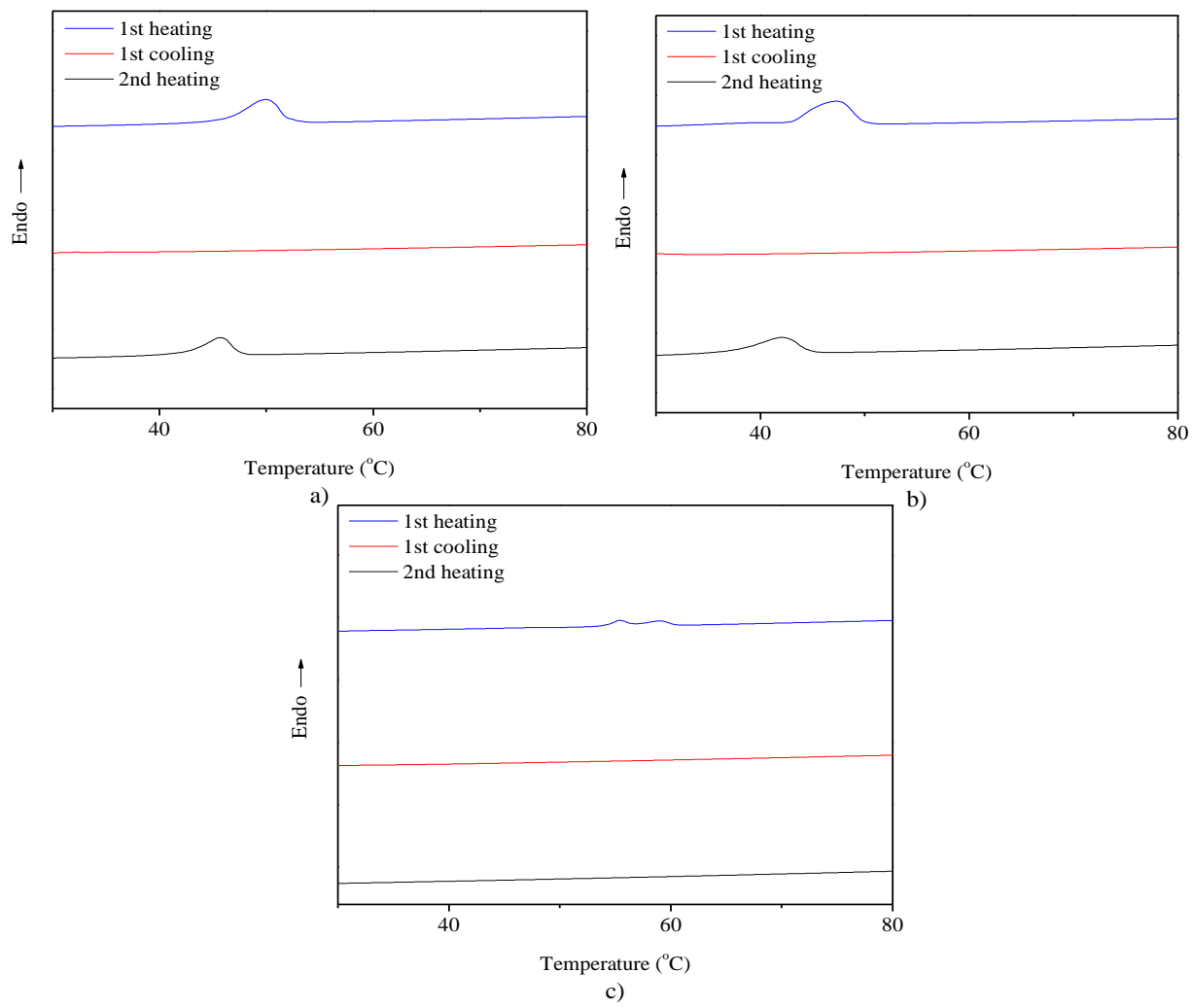


Figure 2.14 DSC of (a) PVL 20:1, (b) PVL 40:1, (c) PU-PVL 20:1.

CHAPTER III
ELECTROSPINNING OF BIODEGRADABLE POLYURETHANES

3.1 Introduction

The electrospun nanofibers with sufficient surface area are of interest due to their ability to mimic tissue-engineering ligament. Electrospinning is a unique technique producing polymeric fibers with diameters ranging from submicron to nanometer scales. There are several advantages to electrospinning, such as the ability to control fiber diameters and morphology^[17]. Therefore, during the electrospinning process, there are several parameters for controlling the morphology of fibers. Generally, these parameters can be divided into three groups, which are polymer solution properties, processing conditions, and ambient conditions. Here, only several parameters are discussed briefly^[48].

Solution viscosity is one of the most important factors among the solution properties. It is easily understood that the viscosity of a solution depends on the change in the molecular weight of polymers. The solution viscosity has been found to increase with increasing the molecular weight of a given polymer^[48]. It is known that a higher molecular weight represents a higher chain length and viscosity, and then the high viscous solution is able to maintain a continuous jet without breaking during electrospinning^[48,49]. If a solution viscosity is too high, then the

electrospinning process may not occur at all, whereas a solution viscosity that is extremely low produces a discontinuous polymer deposition instead of fibers. An appropriate range of solution viscosity is obtained by trial and error.

Surface tension is another main parameter of solution properties. It is generally defined as a property of the surface of a liquid that allows it to resist an external force. At the step of initiating electrospinning, charges on the polymer solution have to be high enough to overcome the surface tension of the solution ^[50]. This will lead to the stretching of solution with reducing beads.

Due to the various surface tensions of polymer solutions, the effect of the applied voltage or the electric field strength has become one of the most studied parameters among the processing conditions ^[48-50]. Once the high voltage is applied during the electrospinning process, the polymer solution then gets charged and overcomes the surface tension resulting in the formation of a Taylor cone. Usually, the higher the applied voltage or electric field strength, the greater the solution stretches out resulting in a reduction of fiber diameter. Also, the higher voltage increases the rate of solvent evaporation and reduces the flight time between the needle tip and the grounded collector. There is no standard value of applied voltage for different polymer solution ^[50].

The impact of distance between the collector and needle tip has been investigated by researchers. The distance between the needle tip and the grounded collector contributes to the fiber morphology by affecting the flight time which ultimately reflects in the fiber diameter ^[50]. As the distance decreases, the flight time also decreases and the electric field strength increases.

In other words, the lower flight time and electric field strength results for no time for solvent to evaporate while traveling, and which ultimately may lead to bead formation of nanofibers.

3.2 Materials and Methods

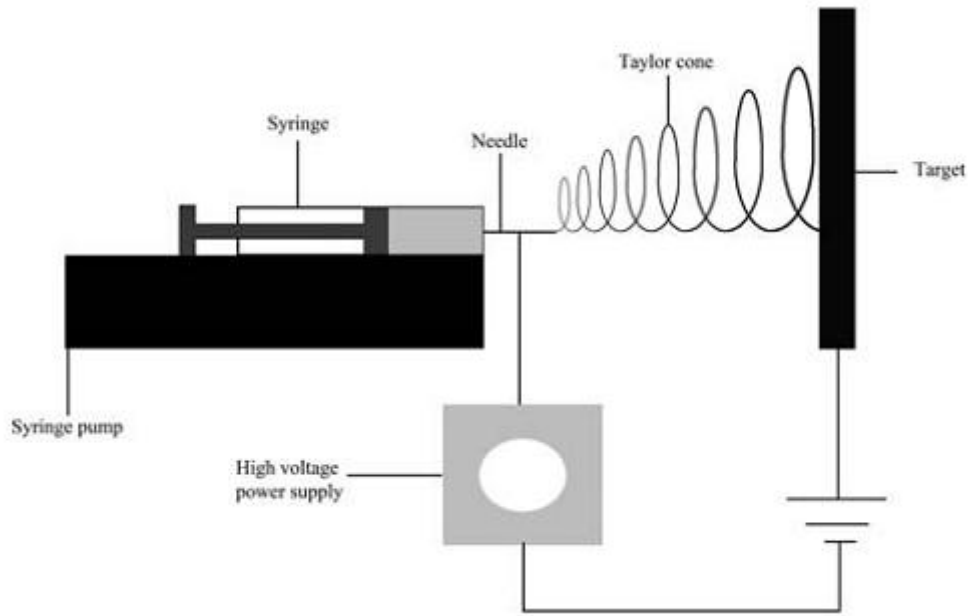
3.2.1 Materials

Phosphate Buffer (pH=7.2), Tetrahydrofuran 99+% (THF) and N, N-dimethylformamide 99.8% (DMF) were purchased from Sigma-Aldrich and used without further purification.

3.2.2 Electrospinning process of PU-PCL and PU-PVL

Polymer solutions were prepared by dissolving the synthesized polyurethanes in a 1:1 THF and DMF mixture under stirring at room temperature. The concentration of polyurethanes solution was initially used as 7.5% wt, 10% wt and 15% wt ^[51]. Each of the samples were vigorously mixed in the presence of a stir bar for at least 2 days and finally the polymer solution was placed in a standard 10 mL glass syringe with a 22 needle gauge (0.7mm OD × 0.4mm ID). The flow rate ranging from 0.01 to 0.02 mL/min was controlled by a KDS syringe pump (KD Scientific Holliston, Inc., MA). The distance between the needle and the grounded collector was kept at a maximum 25cm ^[52]. High voltage power sources, ES30P-5W and ES30N-5W (Gamma High Voltage Research Inc.) for positive and negative voltages respectively, were used to charge the solution in a range of 15-25 kV by attaching the positive electrode to the needle tip through an alligator clip, and the negative electrode to the grounded aluminum mandrel (Scheme 3.1). The electrospun nanofibers were dried under vacuum at room temperature to eliminate the

residual solvent.



Scheme 3.1 The electrospinning set-up ^[52].

3.3 Characterizations

3.3.1 Scanning Electron Microscopy (SEM)

The morphology of electrospun polyurethanes nanofibers was determined by Scanning Electron Microscopy (SEM). Before imaging, the samples were coated by using a thin layer of silver-palladium for a 180 sec for two consecutive cycles at 45mA with the (Desk II Denton Vacuum Cold Sputter). After sample coating, the micrographs from each samples were taken at an accelerating voltage of 15.01 KV. After this sample preparation, the SEM images of samples were obtained in a (SEM) EVO[®] LS10 obtained from (Carl Zeiss SMT., Ltd).

3.3.2 Fourier Transform Infrared Spectroscopy (FT-IR)

FTIR spectra of samples were collected on a Thermo Nicolet Nexus 470 FT-IR spectrometer equipped with a Nexus DTGS detector at room temperature. The scanning numbers were set at 32 under the resolution of 4 cm^{-1} with wavenumbers ranging from $400\text{-}4000\text{ cm}^{-1}$.

3.3.3 Raman spectroscopy

Raman spectra of raw and electrospun samples were compared by Bruker Senterra Optic Raman Microscope. The excitation wavelength was set at 785nm and the laser power to be kept at 50 mW with 50 integrations and 2 co-additions. The spectrum was obtained directly from samples in the region of $400\text{-}3200\text{ cm}^{-1}$.

3.3.4 Thermogravimetric Analysis (TGA)

Electrospun polyurethanes nanofibers samples were placed on a TGA-7 (Perkin Elmer) and heated from 20 to $800\text{ }^{\circ}\text{C}$ at a rate of $10\text{ }^{\circ}\text{C}/\text{min}$ under nitrogen atmosphere.

3.3.5 Differential Scanning Calorimetry (DSC)

DSC studies were performed using a Perkin Elmer DSC 7 under nitrogen with a flow rate of $20\text{ mL}/\text{min}$. The samples were heated from room temperature to $250\text{ }^{\circ}\text{C}$ using alumina pans. The scanning rates were kept as $10\text{ }^{\circ}\text{C}/\text{min}$.

3.3.6 Degradation behavior

Degradation tests were performed in phosphate buffer at pH 7.2. The electrospun nanofiber mats were cut approximate 0.005 grams. The samples were introduced into the phosphate buffer and kept at 37 °C for 5 days. After this, the samples were rinsed using deionized water and dried at 37 °C for 3 days, then weighed again. The same process was repeated every 5 days over 3 weeks. The degradation process was also performed with 4M NaOH for a few seconds before introducing the samples into the phosphate buffer at pH 7.2. This step of placing the samples in 4M NaOH, was deliberated to activate the degradation process so as to observe changes in a shorter period of time.

3.4 Results and Discussions

3.4.1 Electrospinning parameters

Fibrous mats were obtained by electrospinning the synthesized PCL and PVL polyurethanes, which were dissolved in THF and DMF in a ratio of 1:1. The details in processing conditions were listed in Table 3.1. The concentrations of the polymer solutions have been varied due to the difference in molecular weight of obtained polymers.

Table 3.1 Electrospinning conditions of PU-PCL and PU-PVL polymers.

No.	Samples	Concentration (% w/v)	Solvent		Flow rate (mL/min)	Distance (cm)	Voltage (\pm KV)	Remarks
			THF	DMF				
1	PU-PCL	10	THF 50%	DMF 50%	0.02	25	20	Beads
2	PU-PCL	15	THF 50%	DMF 50%	0.01	25	25	Continuous Fiber
3	PU-PVL	20	THF 50%	DMF 50%	0.02	25	25	No fibers

3.4.2 SEM

In the case of PU-PCL, a concentration of 10% (w/v) solution was initially electrospun. The results of electrospun PU-PCL are illustrated in Figure 3.1a with low magnification and Figure 3.1b with high magnification, respectively. In Figure 3.1b, it is observed that a few nanofibers were obtained by electrospinning at the concentration of 10% solution in THF and DMF. However, it also displays many aggregated particles, resulting in a bad morphology of nanofibers. From this figure, it can be explained that the solution concentration of the sample is not high enough to maintain and produce a continuous jet without breaking during electrospinning. In other words, with a low concentration leading to a low viscosity, the discontinuous depositions are able to be produced instead of fibers.

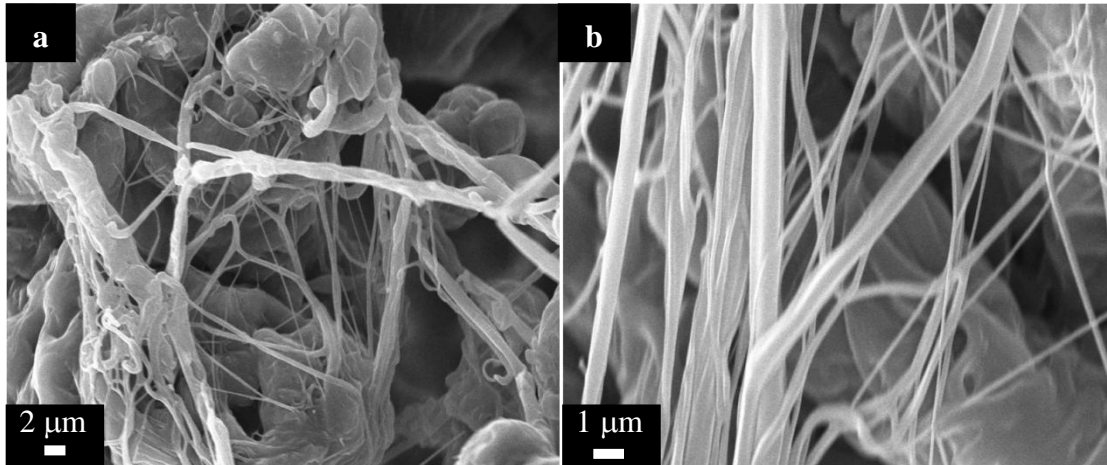


Figure 3.1 SEM micrographs of 10 % (w/v) of PU-PCL nanofibers.

In order to get continuous fibers with a good morphology, the concentration of PU-PCL solution was increased to 15% (w/v). It can be seen in the case of Figure 3.2a-b that electrospun nanofibers are obtained without any defects, as were in the case of 10% wt (Figure 3.1). In more details, it can be seen that the diameter of nanofibers range from 450nm to 2μm at this stage. Comparing to Figure 3.1a, the amount of suspended aggregates decreased dramatically in Figure 3.2a, whereas a higher degree of fiber formation is observed. It is also obvious that there are no beads on the surface of the nanofibers. It is found that by increasing the concentration of the solution, more continuous fibers were obtained finally, which is confirmed with that the concentration is one of the main factors to influence the morphology of electrospun nanofibers. By decreasing the flow rate from 0.02 mL/min to 0.01 mL/min, the solution was jetted continuously without visible dripping out of polymer solution during electrospinning process. The decrease in the flow rate helped in the increase for possibility to maintain the continuous fibers. Furthermore, as the voltage increased, the fibers with low diameters were obtained, which is in agreement with previous literature reports ^[53].

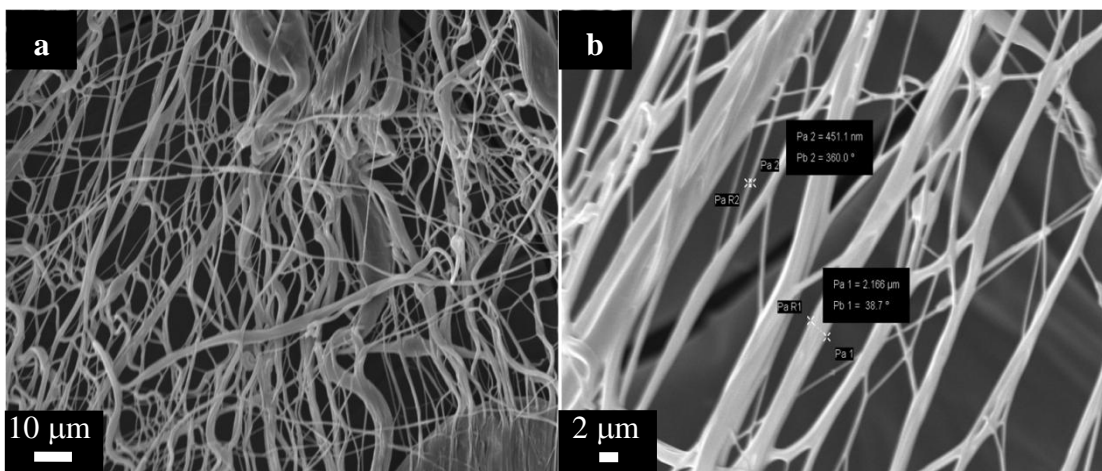


Figure 3.2 SEM micrographs of 15% (w/v) of PU-PCL nanofibers.

Figure 3.3(a-b) represent the SEM images of electrospun polyurethane based on PVL. Based on the SEM images of 15% (w/v) of PU-PCL and the relative low molecular weight of PU-PVL comparing with that of PU-PCL, the first PU-PVL solution in 1:1 ratio of THF and DMF was started at a concentration of 20% (w/v). It was found that, in either low magnification image (Figure 3.3a) or high magnification one (Figure 3.3b), no fibers were observed at a concentration of 20% (w/v), while keeping the same applied voltage, distance between needle tip to collector and flow rate. Instead of fabrication of fibers, the nanoparticles were obtained during the electrospinning. The formation of beads without fibers can be attributed to the nature of the solution obtained by dissolving PU-PVL. The low molecular weight of PU-PVL synthesized in the lab resulted in the low concentration of polymer solution. It is observed that PU-PCL was insoluble in THF during the determination of molecular weight by using SEC. The insolubility of PU-PCL in THF indicated a relatively high molecular weight. In contrast, PU-PVL was soluble in THF with the number average molecular weight of 12,637 g/mol and polydispersity index of 2.27, respectively.

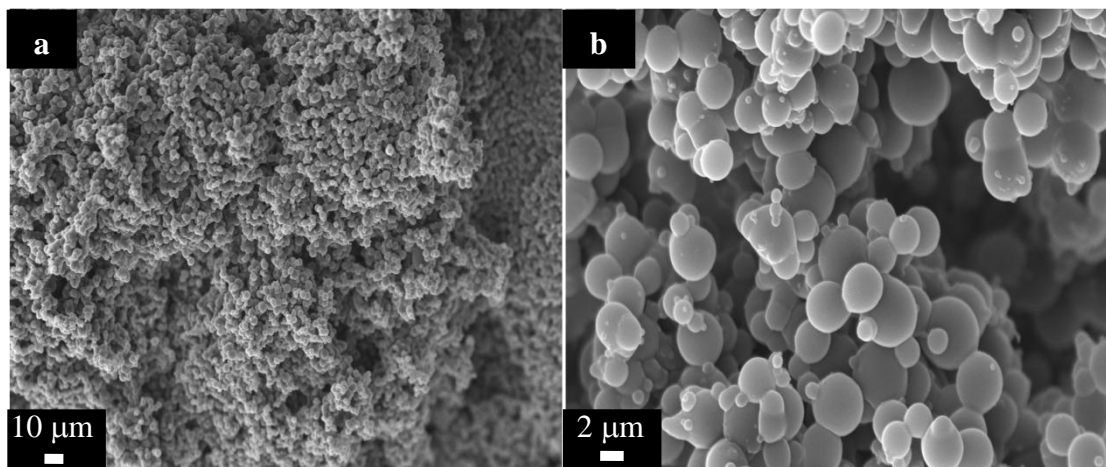


Figure 3.3 SEM micrographs of 20% (w/v) of PU-PVL after electrospinning.

3.4.3 FT-IR spectra

The Fourier transform infrared spectroscopy was utilized to compare the structure of bulk PU-PCL polymer with that of electrospun PU-PCL (Figure 3.4). It can be seen that these spectra are quite similar to each other and the peaks in the region of $1000\text{-}1600\text{ cm}^{-1}$ appear at the same bands. The difference between them is the intensity of some peaks. In addition, the characteristic peaks of electrospun PU-PCL in the region of $1700\text{-}3000\text{ cm}^{-1}$ slightly had shifted. Furthermore, it is observed that the broad peak at 3390 cm^{-1} belonging to N-H stretching (hydrogen bonded+free) had disappeared instead of a very weak intensity.

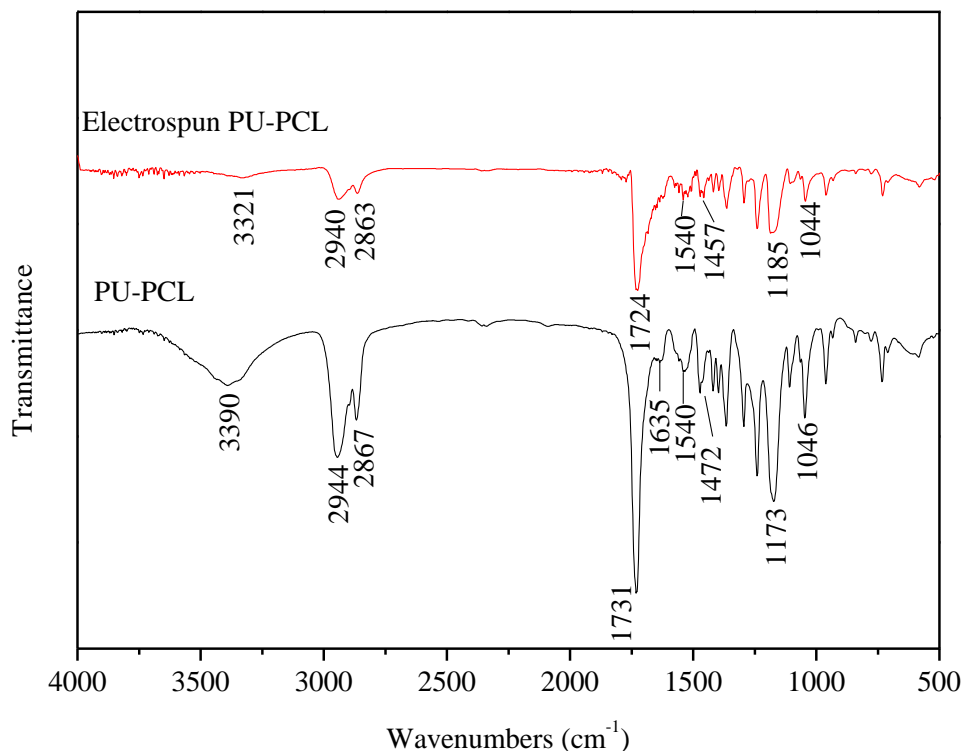


Figure 3.4 FT-IR spectra of bulk PU-PCL and electrospun PU-PCL.

3.4.4 Raman spectra

Raman spectroscopy was used to compare the structure of the bulk polyurethanes with that of the electrospun nanofibers. The spectra obtained are shown in Figure 3.5. The band in the 1722 cm^{-1} region is attributed to the stretching vibration of the C=O groups in the urethane, urea and caprolactone. The frequency of the C=O stretching was maintained in the PU-PCL, as well as on the electrospun PU-PCL nanofibers. Other characteristic bands of CH₂ groups from soft segments and hard segments were found at 2911 cm^{-1} and 2865 cm^{-1} , which are assigned to asymmetric CH₂ stretching and symmetric CH₂ stretching. Peaks at 1440 cm^{-1} and 1304 cm^{-1}

correspond to the CH₂ scissoring and wagging vibrations, respectively. Symmetric and asymmetric stretching vibrations of carbon are observed at 1107 cm⁻¹ and 1063 cm⁻¹. The assignments of Raman spectra for electrospun PU-PCL are tabulated in Table 3.2. It is shown that there is no significant difference observed in the comparison of Raman spectra for PU-PCL and electrospun PU-PCL.

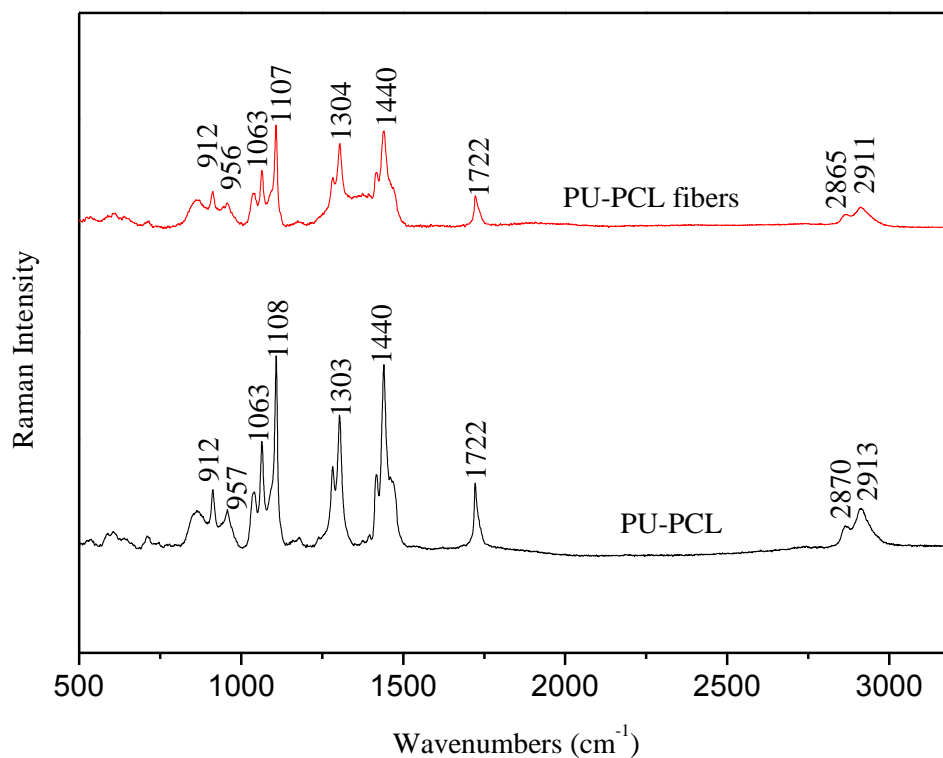


Figure 3.5 Raman spectra of bulk PU-PCL and electrospun PU-PCL.

Table 3.2 Characteristic peak assignments for Raman spectrum of electrospun PU-PCL.

Frequency (cm ⁻¹)	Assignment
2911	Asymmetric CH ₂ stretching
2865	Symmetric CH ₂ stretching
1722	Carbonyl stretching
1440	CH ₂ scissoring
1304	CH ₂ wagging
1107	Symmetric carbon stretching
1063	Asymmetric carbon stretching
912	C-O-C stretching

3.4.5 TGA

The TGA result in Figure 3.6 revealed that the PU-PCL 20:1 and the electrospun PU-PCL decomposed in a single step. However, the onset decomposition temperature for PU-PCL was 337 °C, which was 6 °C lower than that of electrospun PU-PCL corresponding to 342 °C.

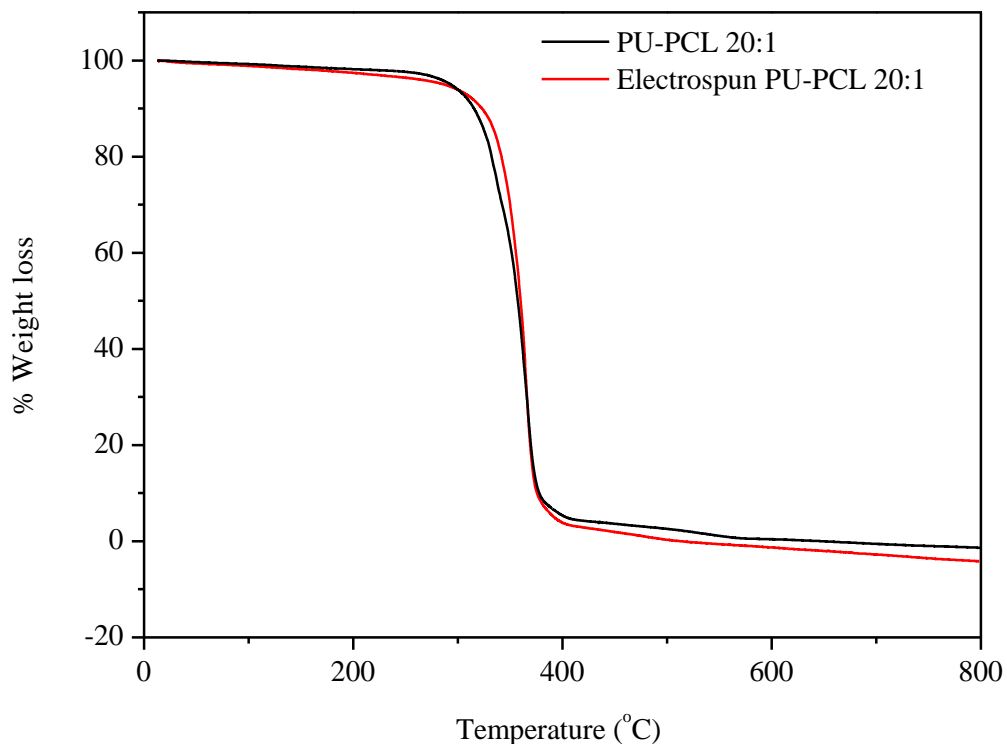


Figure 3.6 TGA curves of PU-PCL 20:1 and electrospun PU-PCL 20:1.

3.4.6 DSC

DSC analysis of electrospun PU-PCL 20:1 nanofibers are presented in Figure 3.7. Two melting points were obtained at 35 °C and 44 °C during the first heating cycle. However, no endothermic peaks were observed at the second heating cycle for electrospun PU-PCL 20:1 nanofibers, indicated that after first melting, the electrospun PU-PCL 20:1 nanofibers were not able to retain the crystallinity. Akcelrud and coworkers attributed the described trend to a more limited mobility for segment crystallization (or a higher viscosity) when PCL was linked to a polymer chain in relation to the free state ^[47].

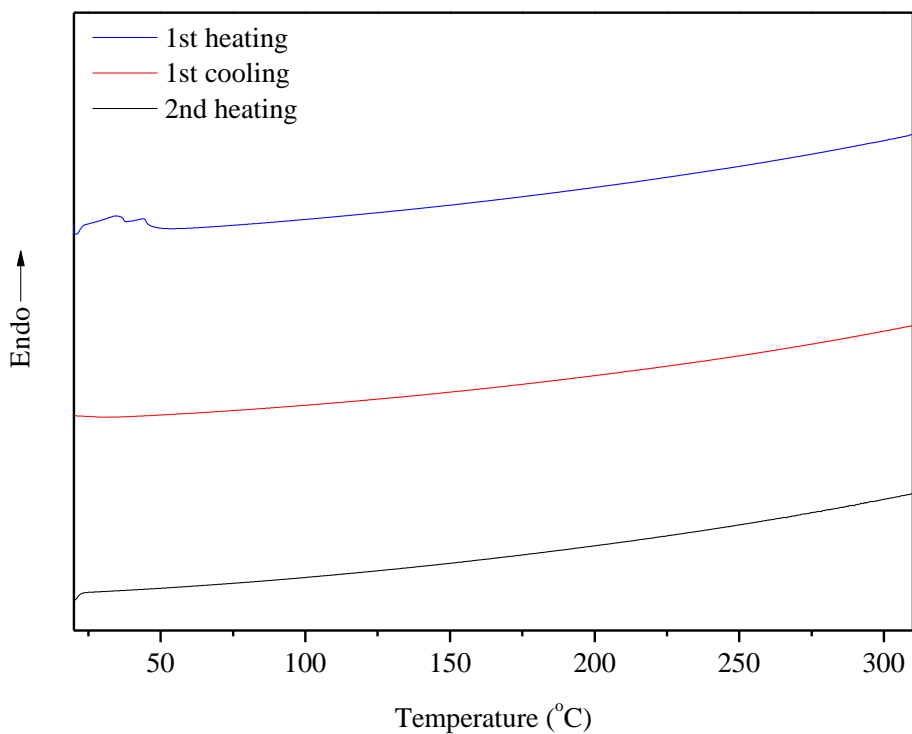


Figure 3.7 DSC curves of electrospun PU-PCL 20:1.

3.4.7 Degradation of electrospun polyurethanes

Electrospun PU-PCLs degradations were measured in phosphate buffer at 37 °C over 3 weeks. The samples (A, B and C) were immersed in 4M NaOH for a few seconds before placing into buffer. The weight numbers and degradation (%) were listed in Table 3.3. The calculations of means and standard deviations were shown in Appendix. On the other hand, samples (E, F and G) were directly introduced into buffer. The collected data were tabulated in Table 3.4.

Table 3.3 Electrospun PU-PCLs (A, B and C) were immersed in 4M NaOH before placing into phosphate buffer.

Week		0	1	2	3
A	Weight (mg)	5.75	5.47	5.32	4.76
	Degradation (%)	0.00	4.87	7.48	17.22
B	Weight (mg)	5.52	5.48	5.48	5.49
	Degradation (%)	0.00	0.72	0.72	0.54
C	Weight (mg)	4.59	4.59	4.54	4.59
	Degradation (%)	0.00	0.00	1.09	0.00
Mean (%)		0.00	1.86	3.10	5.92
Standard Deviation (%)		0.00	2.63	3.80	9.79

Degradation curves of electrospun PU-PCL were presented in Figure 3.8 or (Figure 3.9 & Figure 3.10). As can be seen, both cases exhibited certain weight loss over 3 weeks after degradation. As for those samples (A, B and C) immersed in 4M NaOH, an initial 1.8% degradation was observed, and then the weight was continued dropping and ended up at 5.9% with a distinct decrease in weight loss. However, for those samples (E, F and G) without immerse in NaOH, it is shown that an initial 2.9% degradation was higher than the one in terms of degradation with samples (A, B and C). It is also found that after 1 week, the trend of degradation was kept at around 2.9% at a period of 3 weeks. Regarding the degradation weeks, long periods of degradation studies are necessary to be continued and investigated.

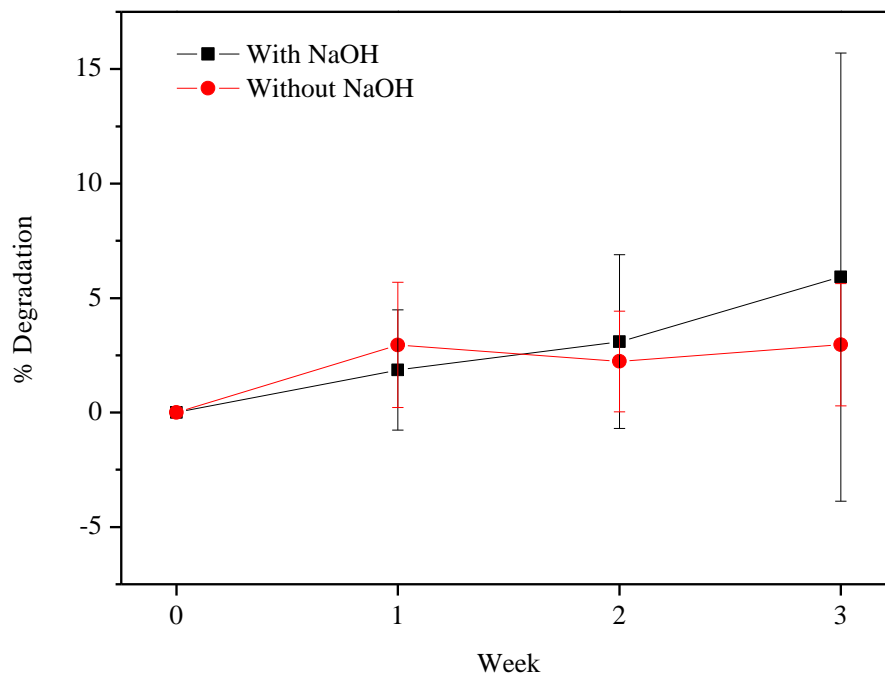


Figure 3.8 Degradation curves of electrospun PU-PCLs in phosphate buffer (pH=7.2) at 37 °C.

All values are mean \pm SD, $n=3$.

Table 3.4 Electrospun PU-PCLs (E, F and G) were in Phosphate buffer.

week		0	1	2	3
E	Weight (mg)	5.00	4.73	4.78	4.74
	Degradation (%)	0.00	5.40	4.40	5.20
F	Weight (mg)	3.78	3.78	3.78	3.78
	Degradation (%)	0.00	0.00	0.00	0.00
G	Weight (mg)	4.35	4.20	4.25	4.19
	Degradation (%)	0.00	3.45	2.30	3.68
Mean (%)		0.00	2.95	2.23	2.96
Standard Deviation (%)		0.00	2.73	2.20	2.67

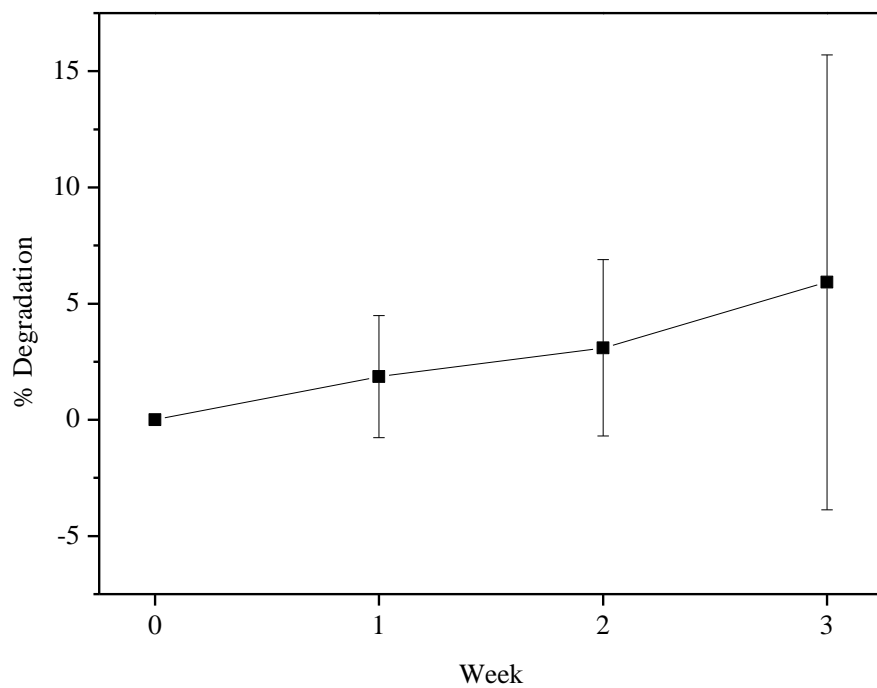


Figure 3.9 Degradation of electrospun PU-PCLs (A, B and C) immersed in 4M NaOH before placing into phosphate buffer (pH=7.2) at 37 °C. All values are mean \pm SD, $n=3$.

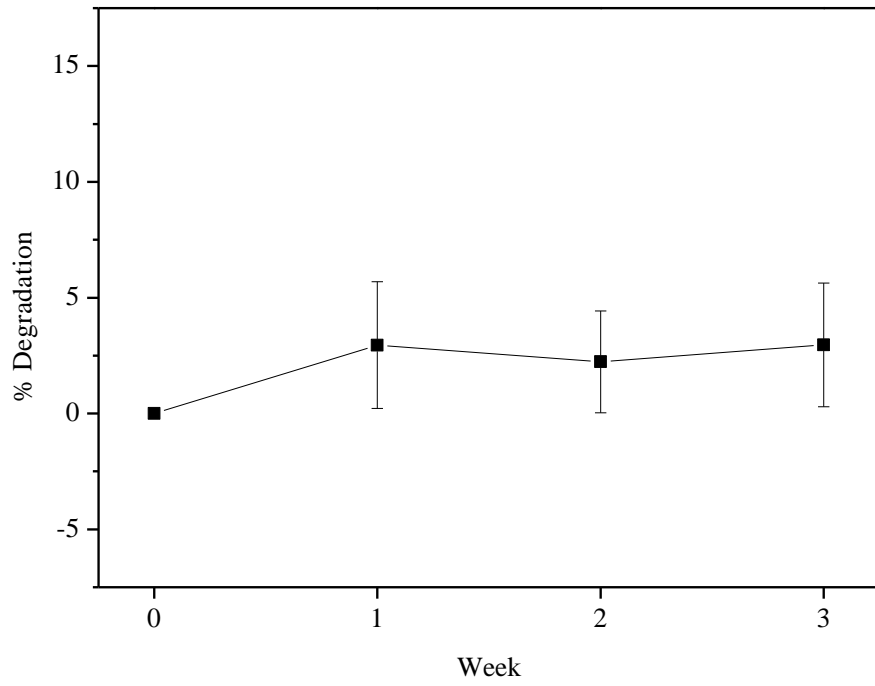


Figure 3.10 Degradation of electrospun PU-PCLs (E, F and G) placing into phosphate buffer (pH=7.2) at 37 °C. All values are mean \pm SD, $n=3$.

CHAPTER IV

CONCLUSIONS AND FUTURE WORK

4.1 Conclusions

In this study, poly(ϵ -caprolactone) (PCL) and poly(δ -valerolactone) (PVL) were successfully synthesized. In each case, the syntheses of polymers were carried out by ring-opening polymerization of ϵ -caprolactone (CL) and δ -valerolactone (VL) with diethylene glycol (DEG) as an initiator and stannous octoate as a catalyst. Low molecular weights of PCL (4,844 g/mol and 5,827 g/mol) and PVL (5,868 g/mol and 4,218 g/mol) were obtained and corroborated by ^1H NMR and SEC. Meanwhile, by changing the monomer to initiator (M/I) ratio, a unique trend on molecular weights was observed. It indicated that as the M/I ratio increases, the molecular weight for PCL increases, whereas the molecular weight of PVL decreases. From these reactions and obtained values of molecular weights, the poly(ϵ -caprolactone) is preferred to be used for synthesis of polyurethane. Furthermore, thermal analysis depicts that the onset temperature is 310 $^{\circ}\text{C}$ for PCL and 290 $^{\circ}\text{C}$ for PVL. While, the melting points were around 50 $^{\circ}\text{C}$ and 53 $^{\circ}\text{C}$ for PCL with two endothermic peaks but only one endothermic peak was seen at 50 $^{\circ}\text{C}$ for PVL.

We also conclude that the syntheses of polyurethane based on obtained poly(ϵ -caprolactone) (PU-PCL) and poly(δ -valerolactone) (PU-PVL) were successful by using a two-step reaction

method with 1,4-diisocyanatebutane (BDI) and 1,4-diaminobutane (putrescine) as a chain extender. SEC results showed a molecular weight of 12,627 g/mol for PU-PVL. However, the molecular weight for PU-PCL was relatively high, confirmed with its insolubility in THF in SEC. Thermal results demonstrate that the onset temperature for PU-PCL was 337 °C with a 27 °C increase comparing to PCL. As for PU-PVL, the onset temperature was 10 °C higher than PVL.

In the study of electrospinning, synthesized PU-PCL nanofibers were successfully fabricated by this technique. However, in the case for electrospinning of PU-PVL, beads were produced instead of nanofibers. SEM images revealed a good morphology of electrospun PU-PCL nanofibers at a concentration of 15% (w/v) in THF and DMF as 1:1 ratio. The bulk PU-PCL and electrospun PU-PCL nanofibers showed a single melting peak almost at 337 °C and 342 °C, respectively from DSC results. Two endothermic peaks were observed at 35 °C and 44 °C during the first heating for electrospun PU-PCL nanofibers. Characterization of the electrospun PU-PCL nanofibers was also achieved via FT-IR and Raman spectroscopy that revealed no significant difference occurred with regard to the structures of bulk PU-PCL and electrospun PU-PCL nanofibers.

4.2 Future work

More researches will be studied on the synthesis of poly(ϵ -caprolactone) with a high molecular weight. Then, the PCL with high molecular weight will be continuously used for synthesizing different polyurethanes. Higher molecular weights will help to obtain enhanced thermal stability and mechanical properties. Once the higher molecular weight polyurethanes are

achieved, these will be compared with commercially available polyurathanes, like Lycra, Biospan, Tecoflex and Carbothanes. The tailored polyurethanes will be selected to do electrospinning, so as to have nanofibers with robust mechanical properties. Finally, biodegradability needs to be tested in different conditions to figure out the degradation.

REFERENCES

1. Petrigliano, F. & McAllister, D. Tissue engineering for anterior cruciate ligament reconstruction: a review of current strategies. *Arthroscopy: The Journal of Arthroscopic and Related Surgery* **22**, 441-451 (2006).
2. Freeman, J. Recent advancements in ligament tissue engineering: the use of various techniques and materials for ACL repair. *Recent Patents on Biomedical Engineering* **1**, 18-23 (2008).
3. Vunjak-Novakovic, G. & Altman, G. Tissue engineering of ligaments. *Tissue Engineering for Tissue and Organ Regeneration* **8**, (2004).
4. Laurencin, C. Ligament tissue engineering: an evolutionary materials science approach. *Biomaterials* **26**, 7530-7536 (2005).
5. Liljensten, E. & Edberg, B. Studies of polyurethane urea bands for ACL reconstruction. *Journal of materials science. Materials in medicine* **13**, 351-9 (2002).
6. Christian, P., Jones, I. & Rudd, C. Monomer transfer moulding and rapid prototyping methods for fibre reinforced thermoplastics for medical applications. *Composites Part A* **32**, 969-976 (2001).
7. Cooper, J. a, Lu, H.H., Ko, F.K., Freeman, J.W. & Laurencin, C.T. Fiber-based tissue-engineered scaffold for ligament replacement: design considerations and in vitro evaluation. *Biomaterials* **26**, 1523-32 (2005).
8. Prabhakar, R.L., Brocchini, S. & Knowles, J.C. Effect of glass composition on the degradation properties and ion release characteristics of phosphate glass--polycaprolactone composites. *Biomaterials* **26**, 2209-18 (2005).
9. Sahoo, S., Ouyang, H., Goh, J.C.-H., Tay, T.E. & Toh, S.L. Characterization of a novel polymeric scaffold for potential application in tendon/ligament tissue engineering. *Tissue engineering* **12**, 91-9 (2006).

10. Kuo, C. & Marturano, J. Novel strategies in tendon and ligament tissue engineering: Advanced biomaterials and regeneration motifs. *Sports Medicine, Arthroscopy, Rehabilitation, Therapy & Technology* **2**, (2010).
11. Lemos, V. a. *et al.* Application of polyurethane foam as a sorbent for trace metal pre-concentration — A review. *Spectrochimica Acta Part B: Atomic Spectroscopy* **62**, 4-12 (2007).
12. Gogolewski, S. Selected topics in biomedical. *Colloid & Polymer Science* **785**, 757-785 (1989).
13. Howard, G.T. Biodegradation of polyurethane: a review. *International Biodeterioration & Biodegradation* **49**, 245-252 (2002).
14. Guan, J. Synthesis, characterization and cytocompatibility of polyurethaneurea elastomers with designed elastase sensitivity. *Biomacromolecules* **6**, 2833-2842 (2005).
15. Mishra, A., Chattopadhyay, D.K. & Sreedhar, B. FT-IR and XPS studies of polyurethane-urea-imide coatings. *Progress in Organic Coatings* **55**, 231-243 (2006).
16. Boudriot, U., Dersch, R. & Greiner, A. Electrospinning Approaches Toward Scaffold Engineering — A Brief Overview. *Artificial Organs* **30**, 785-792 (2006).
17. Subbiah, T., Bhat, G. & Tock, R. Electrospinning of nanofibers. *Journal of Applied Polymer Science* **96**, (2005).
18. Reneker, D.H. & Yarin, A.L. Electrospinning jets and polymer nanofibers. *Polymer* **49**, 2387-2425 (2008).
19. Taylor, G. Electrically driven jets. *Proceedings of the Royal Society of London. Series A, Mathematical and Physical Sciences* **313**, 453-475 (1969).
20. Garg, K. Electrospinning jets and nanofibrous structures. *Biomicrofluidics* **5**, 1-19 (2011).
21. Liang, D. & Hsiao, B. Functional electrospun nanofibrous scaffolds for biomedical applications. *Advanced Drug Delivery Reviews* **59**, 1392-1412 (2007).
22. Kanani, A. Review on electrospun nanofibers scaffold and biomedical applications. *Trends in Biomaterials and Artificial* **24**, 93-115 (2010).

23. Sheikh, F., Barakat, N. & Kanjwal, M. Self synthesise of silver nanoparticles in/on polyurethane nanofibers: Nano - biotechnological approach. *Journal of Applied Polymer Science* **115**, 3189-3198 (2010).
24. Ashammakhi, N., Ndreu, A. & Yang, Y. Nanofiber-based scaffolds for tissue engineering. *European Journal of Plastic Surgery* **35**, 135-149 (2012).
25. Ramakrishna, S., Mayer, J. & Wintermantel, E. Biomedical applications of polymer-composite materials: a review. *Composites Science and Technology* **61**, 1189-1224 (2001).
26. Tian, H., Tang, Z., Zhuang, X. & Chen, X. Biodegradable synthetic polymers: Preparation, functionalization and biomedical application. *Progress in Polymer Science* **37**, 237-280 (2011).
27. Rezwan, K., Chen, Q.Z., Blaker, J.J. & Boccaccini, A.R. Biodegradable and bioactive porous polymer/inorganic composite scaffolds for bone tissue engineering. *Biomaterials* **27**, 3413-31 (2006).
28. Gunatillake, P. & Adhikari, R. Biodegradable synthetic polymers for tissue engineering. *European Cells and Materials* **5**, 1-16 (2003).
29. Jagur-Grodzinski, J. Biomedical application of functional polymers. *Reactive and Functional Polymers* **39**, 99-138 (1999).
30. Woodruff, M. The return of a forgotten polymer — Polycaprolactone in the 21st century. *Progress in Polymer Science* **35**, 1217-1256 (2010).
31. Ping, P., Wang, W. & Chen, X. Poly (ϵ -caprolactone) polyurethane and its shape-memory property. *Biomacromolecules* **6**, 587-592 (2005).
32. Storey, R.F. & Sherman, J.W. Kinetics and Mechanism of the Stannous Octoate-Catalyzed Bulk Polymerization of ϵ -Caprolactone. *Macromolecules* **35**, 1504-1512 (2002).
33. Guan, J., Fujimoto, K. & Sacks, M. Preparation and characterization of highly porous, biodegradable polyurethane scaffolds for soft tissue applications. *Biomaterials* **26**, 3961-3971 (2005).
34. Arcana, I., Bundjali, B. & Hasan, M. The effect of the soft segment of prepolymers on properties of poly (urethane - ester) and its biodegradability. *Polymer International* **60**, 1535-1540 (2011).

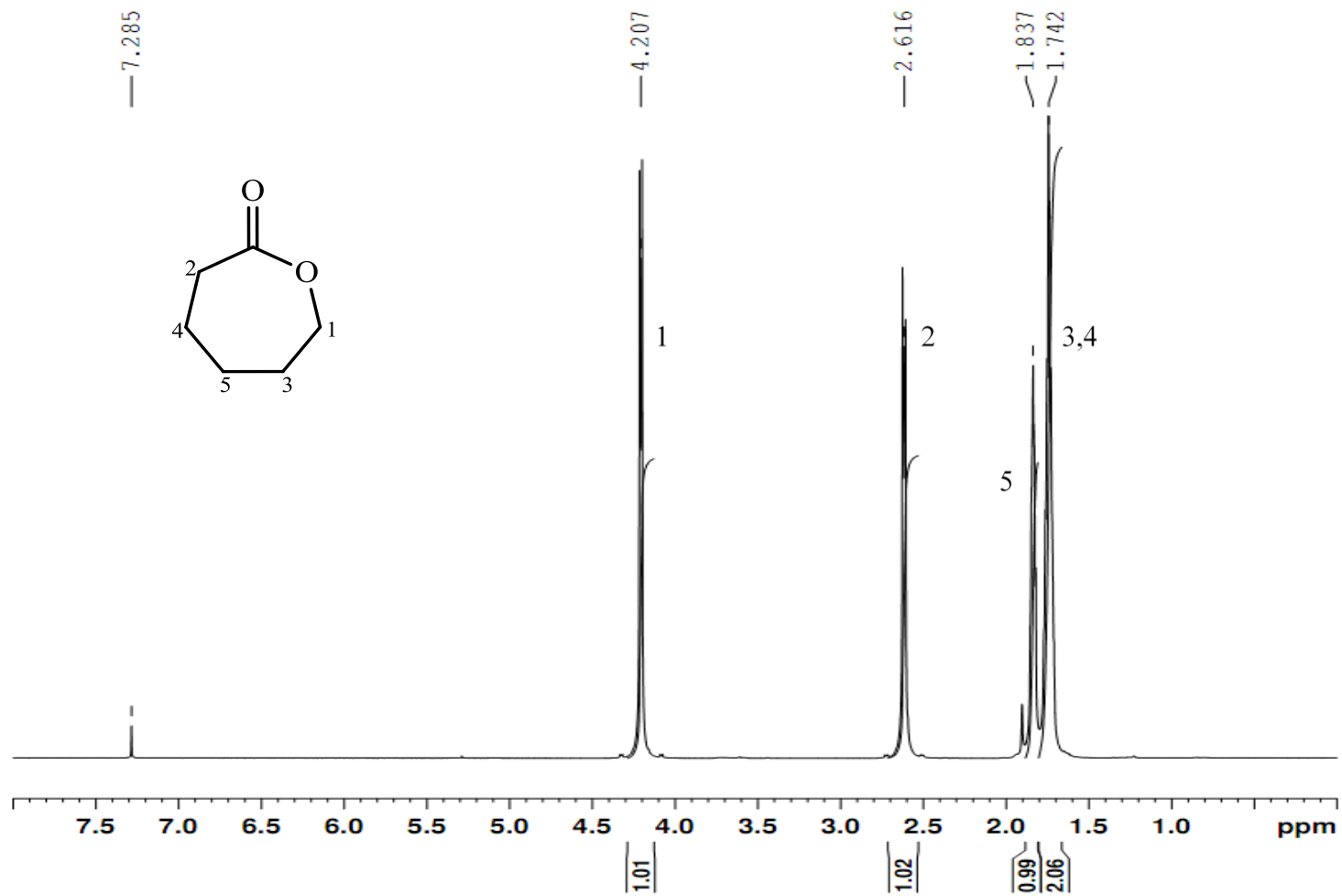
35. Elzein, T., Nasser-Eddine, M., Delaite, C., Bistac, S. & Dumas, P. FTIR study of polycaprolactone chain organization at interfaces. *Journal of colloid and interface science* **273**, 381-7 (2004).
36. Gorna, K. & Gogolewski, S. In vitro degradation of novel medical biodegradable aliphatic polyurethanes based on ϵ -caprolactone and Pluronic® with various hydrophilicities. *Polymer Degradation and Stability* **75**, 113-122 (2002).
37. Ryszkowska, J.L., Auguścik, M., Sheikh, A. & Boccaccini, A.R. Biodegradable polyurethane composite scaffolds containing Bioglass® for bone tissue engineering. *Composites Science and Technology* **70**, 1894-1908 (2010).
38. Krishnan, K. Raman and infrared spectra of ethylene glycol. *Proceedings of the Indian Academy of Sciences, Section A* **2**, 111-123 (1966).
39. Foggia, M.D., Corda, U., Plescia, E. & Taddei, P. Effects of sterilisation by high-energy radiation on biomedical poly-(ϵ -caprolactone)/hydroxyapatite composites. *Journal of Materials Science: Materials in Medicine* **21**, 1789-1797 (2010).
40. Rockwood, D. & Woodhouse, K. Characterization of biodegradable polyurethane microfibers for tissue engineering. *Journal of Biomaterials Science, Polymer Edition* **18**, 743-758 (2007).
41. Kazuo, S. & Yasuto, K. Polymerization of δ - valerolactone and preparation of a thermostable derivative from its polyester. *Die Makromolekulare Chemie* **82**, 41-52 (1965).
42. Vivas, M., Mejías, N. & Contreras, J. Ring-opening polymerization of lactones initiated by diphenylzinc-coinitiator systems. *Polymer International* **52**, 1005-1009 (2003).
43. Ito, K., Tomida, M. & Yamashita, Y. Ring-chain equilibrium in the anionic polymerization of δ -valerolactone. *Polymer Bulletin* **1**, 569-573 (1979).
44. Saiyasombat, W. *et al.* Ring strain and polymerizability of cyclic esters. *Polymer* **39**, 5581-5585 (1998).
45. Mondal, S. & Martin, D. Hydrolytic degradation of segmented polyurethane copolymers for biomedical applications. *Polymer Degradation and Stability* **2**, (2012).
46. Loh, X.J., Colin Sng, K.B. & Li, J. Synthesis and water-swelling of thermo-responsive poly(ester urethane)s containing poly(epsilon-caprolactone), poly(ethylene glycol) and poly(propylene glycol). *Biomaterials* **29**, 3185-3194 (2008).

47. Kloss, J. *et al.* Poly(ester urethane)s with polycaprolactone soft segments: A morphological study. *Journal of Polymer Science Part A: Polymer Chemistry* **40**, 4117-4130 (2002).
48. Pham, Q. & Sharma, U. Electrospinning of polymeric nanofibers for tissue engineering applications: a review. *Tissue engineering* **12**, (2006).
49. Li, D. Electrospinning of nanofibers: Reinventing the wheel? *Advanced Materials* **16**, 1151-1170 (2004).
50. Bhardwaj, N. Electrospinning: a fascinating fiber fabrication technique. *Biotechnology advances* **28**, 325-347 (2010).
51. Carrizales, C., Pelfrey, S. & Rincon, R. Thermal and mechanical properties of electrospun PMMA, PVC, Nylon 6, and Nylon 6, 6. *Polymers for Advanced Technologies* **19**, 124-130 (2008).
52. Pelfrey, S., Cantu, T. & Papantonakis, M. Microscopic and spectroscopic studies of thermally enhanced electrospun PMMA micro-and nanofibers. *Polymer Chemistry* **1**, 866-869 (2010).
53. Macossay, J., Marruffo, A., Rincon, R., Eubanks, T. & Kuang, A. Effect of needle diameter on nanofiber diameter and thermal properties of electrospun poly(methyl methacrylate). *Polymers for Advanced Technologies* **18**, 180-183 (2007).

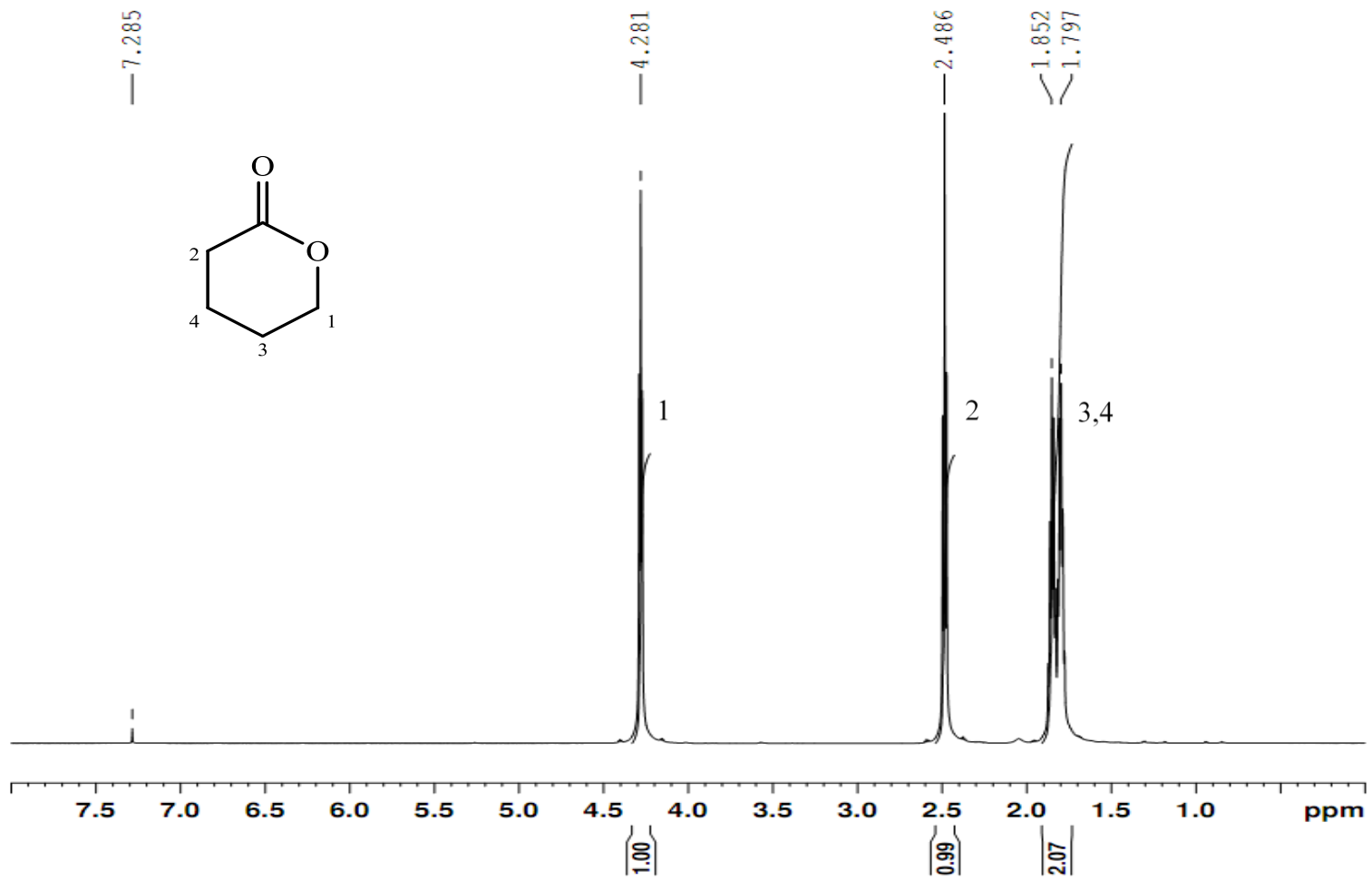
APPENDIX A

APPENDIX A

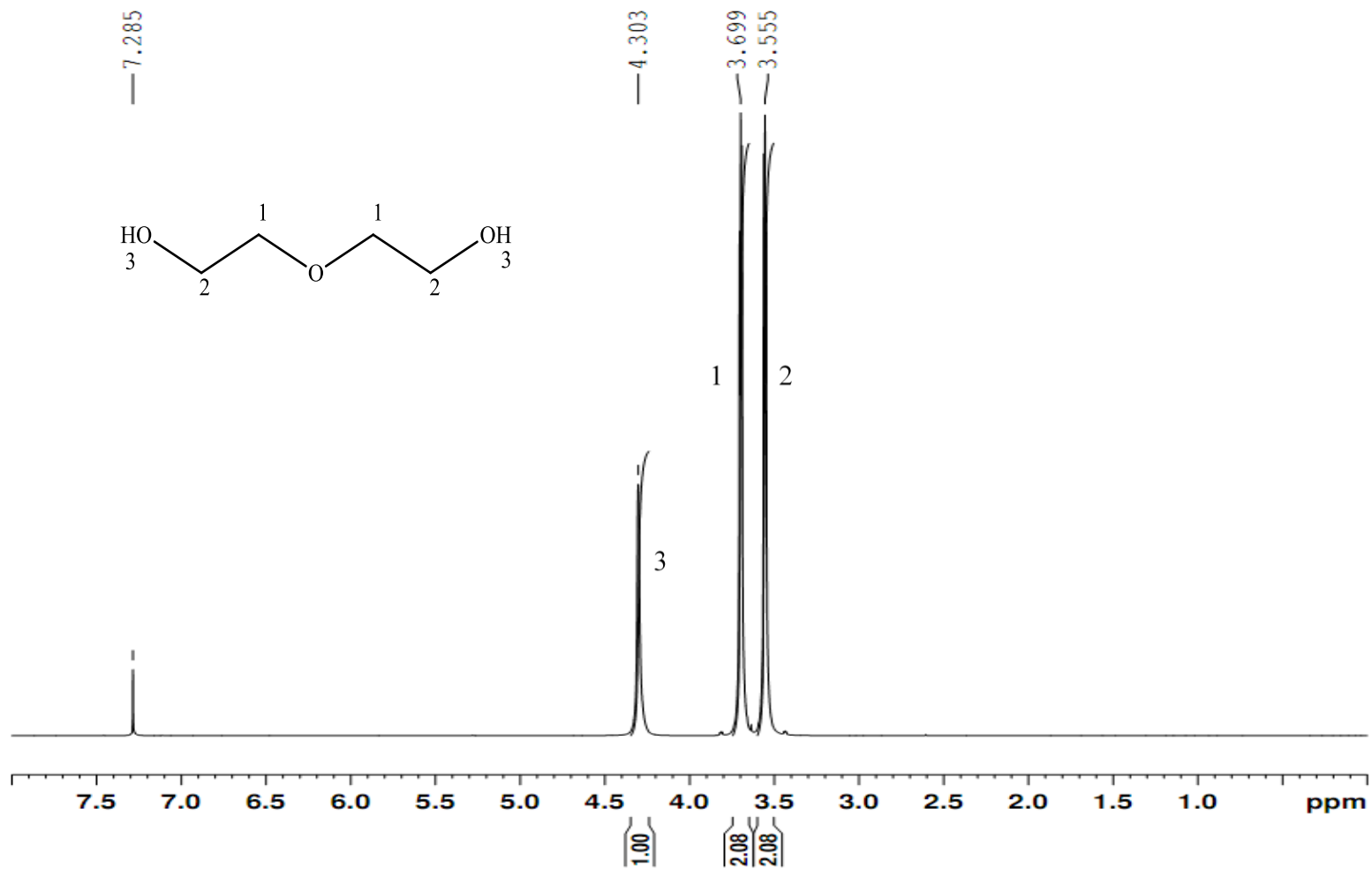
¹H NMR SPECTRA OF STARTING MATERIALS AND CALCULATIONS OF STANDARD DEVIATIONS



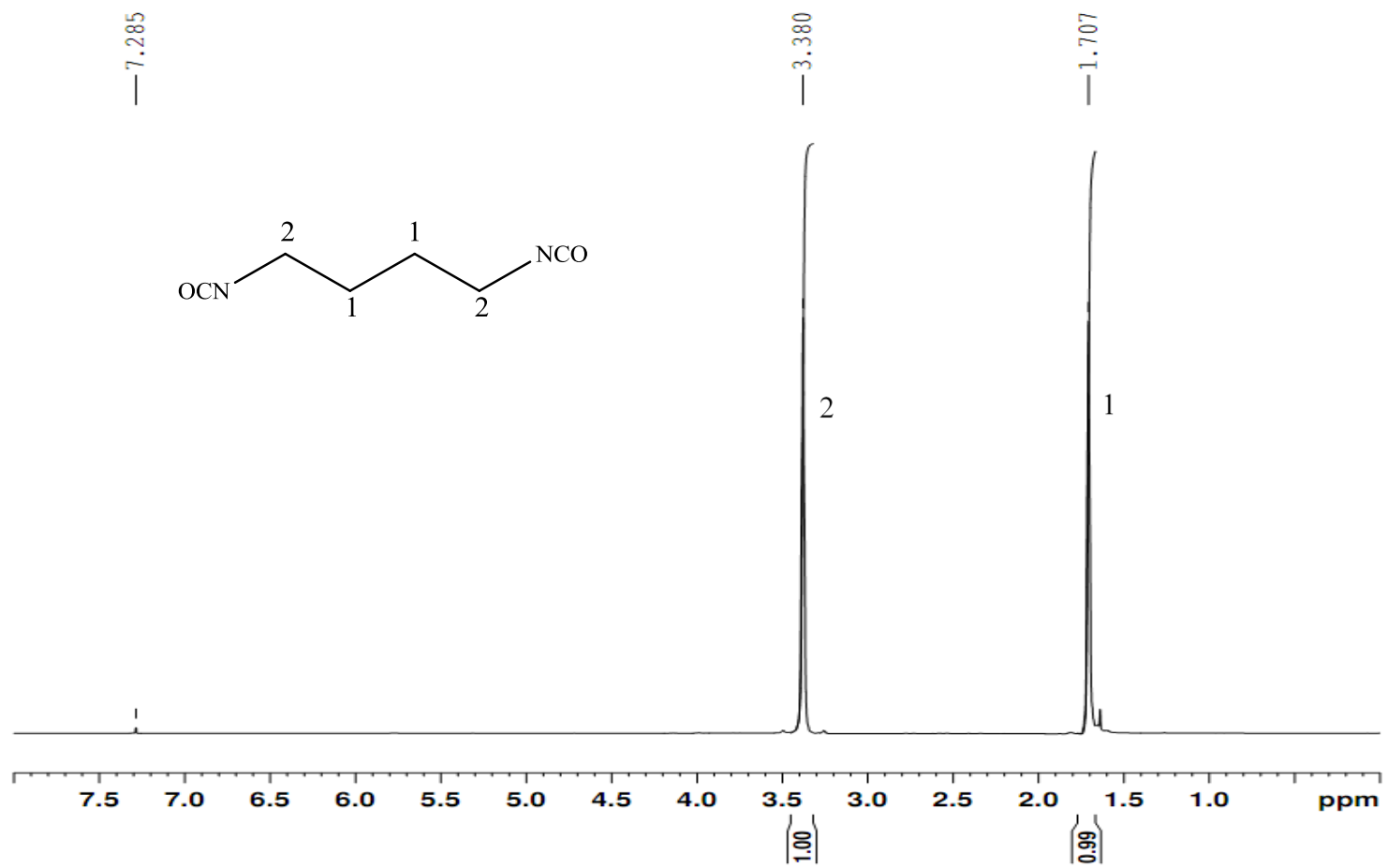
^1H NMR spectrum of ϵ -Caprolactone.



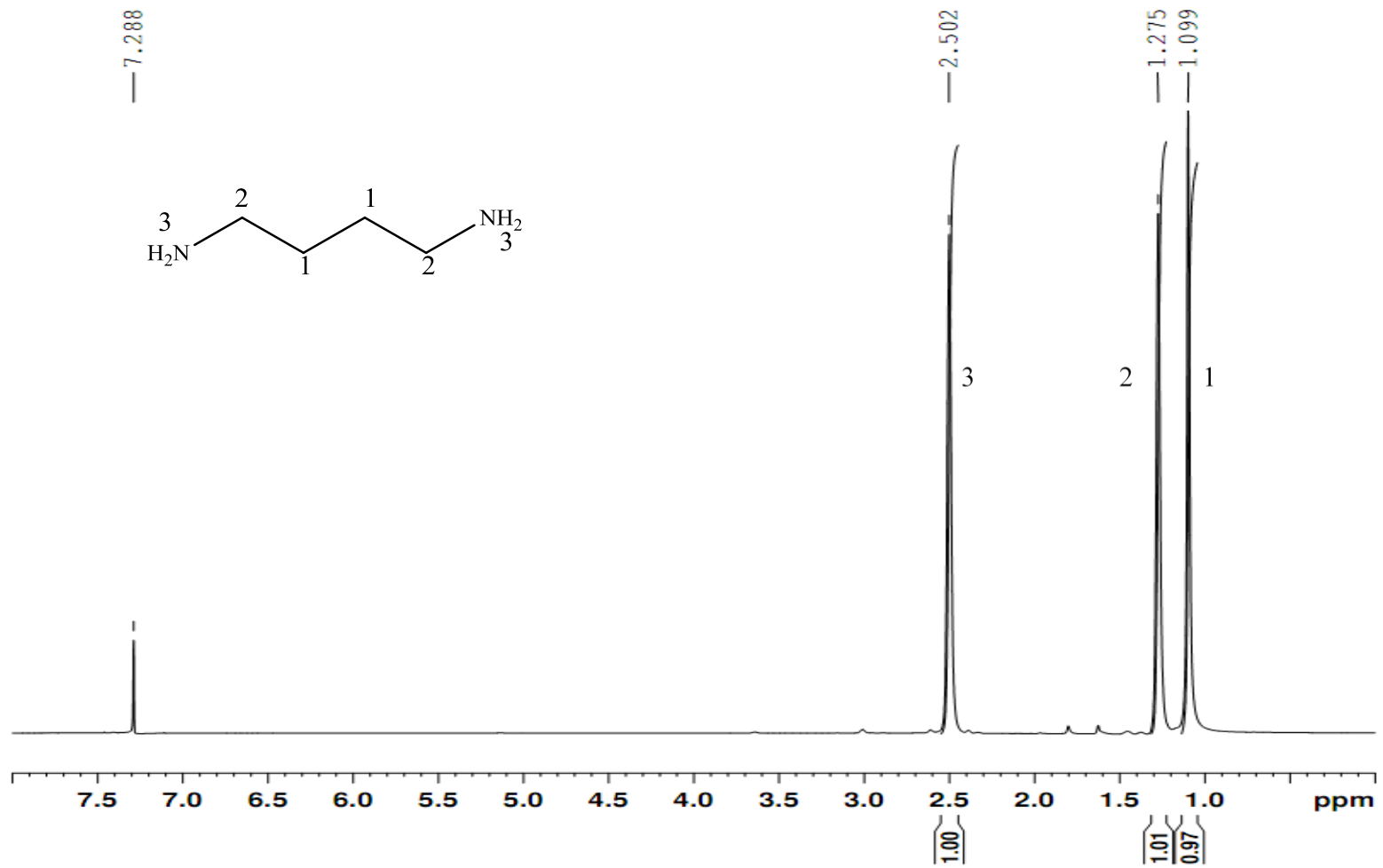
^1H NMR spectrum of δ -valerolactone.



^1H NMR spectrum of diethylene glycol.



^1H NMR spectrum of 1,4-diisocyanate butane (BDI).



^1H NMR spectrum of 1,4-diamino butane (putrescine).

Calculations of degradation (X_i %), mean number of degradation (μ %), standard deviation (σ)

As an example of sample A (TABLE 1,), calculation of the degradation (X_{A1} %) for 1 week as follows, assuming a_0 as starting weight number and a_1 as weight number after 1 week.

$$X_i = \frac{a_1 - a_0}{a_0} \times 100\% = \frac{5.75 - 5.47}{5.75} \times 100\% = 4.87\%$$

Calculation of the mean of degradation and standard deviation for samples (A, B and C) over 1 week as follows.

$$\mu_x = \frac{\sum_{i=1}^n X_i}{n} = \frac{X_{A1} + X_{B1} + X_{C1}}{3} = \frac{4.87\% + 0.72\% + 0\%}{3} = 1.86\%$$

$$\sigma_x = \sqrt{\frac{\sum_{i=1}^n (X_i - \mu_x)^2}{n-1}} = \sqrt{\frac{(4.87\% - 1.86\%)^2 + (0.72\% - 1.86\%)^2 + (0\% - 1.86\%)^2}{3-1}} = 2.63\%$$

X_i degradation (%)

μ mean number of degradation (%)

σ standard deviation

BIOGRAPHICAL SKETCH

Xujun Zhang was born in 1987 in Shanghai. Nineteen years later he entered Shanghai University as an undergraduate studying at the Department of Chemistry. In 2009, he completed his Bachelor of Science in Applied Chemistry. After one year, he started his graduate studies at the University of Texas-Pan American to pursue his Master of Science degree. In 2012, he plans to earn a Ph.D at Louisiana State University.

Email address: xnzhang@broncs.utpa.edu